Geoscientific
Model Development
Discussions

# The Cloud_cci simulator for the ESA Cloud_cci climate data record and its application to a global and a regional climate model

Salomon Eliasson[1], Karl Göran Karlsson[1], Erik van Meijgaard[2], Jan Fokke Meirink[2], Martin Stengel[3], and Ulrika Willén[1]

[1]Swedish Meteorological and Hydrological Institute (SMHI)
[2]Koninklijk Nederlands Meteorologisch Instituut (KNMI)
[3]Deutscher Wetterdienst (DWD)

**Correspondence:** Salomon Eliasson (salomon.eliasson@smhi.se)

**Abstract.**

The Cloud Climate Change Initiative (Cloud_cci) satellite simulator has been developed to enable comparisons between the Cloud_cci Climate Data Record (CDR) and climate models. The Cloud_cci simulator is applied here to the EC-Earth Global Climate Model as well as the Regional Atmospheric Climate Model (RACMO) Regional Climate Model. We demonstrate the

5  importance of using a satellite simulator that emulates the retrieval process underlying the CDR as opposed to taking the model output directly. The impact of not sampling the model at the local overpass time of the polar-orbiting satellites used to make the dataset was shown to be large, yielding up to $100\,\%$ error in Liquid Water Path (LWP) simulations in certain regions. The simulator removes all clouds with optical thickness smaller than 0.2 to emulate the Cloud_cci CDR's lack of sensitivity to very thin clouds. This reduces Total Cloud Fraction (TCF) globally by about $10\,\%$ for EC-Earth and by a few percent for RACMO

10  over Europe. Globally, compared to the Cloud_cci CDR, EC-Earth is shown to be mostly in agreement on the distribution of clouds and their height, but it generally underestimates the high cloud fraction associated with tropical convection regions, and overestimates the occurrence and height of clouds over the Sahara and the Arabian sub-continent. In RACMO, TCF is higher than retrieved over the northern Atlantic Ocean, but lower than retrieved over the European continent, where in addition the Cloud Top Pressure (CTP) is underestimated. The results shown here demonstrate again that a simulator is needed to make

15  meaningful comparisons between modelled and retrieved cloud properties. It is promising to see that for (nearly) all cloud properties the simulator improves the agreement of the model with the satellite data.

## 1 Introduction

Clouds have a critical impact on the Earth's radiative budget and its hydrological cycle, yet clouds also present the largest source of uncertainties in climate models (Zelinka et al., 2017). Therefore, in order to increase the fidelity of a model's ability

20  to predict a future climate, a realistic representation of clouds is needed. Indeed, for decades the representation of clouds in models has improved to the degree that we can now make confident statements on the overall cloud-feedback response to a changing climate (Klein et al., 2013; Zelinka et al., 2017). This improvement has for a considerable part been enabled by the increased availability of global satellite measurements of clouds. However, despite that great strides have been made in

improving the representation of clouds since the Intergovernmental Panel on Climate Change (IPCC)'s first assessment report, they still constitute one of the main challenges to climate modelling (Stocker et al., 2013).

More than 30 years ago, to improve weather forecasts operational weather satellites were launched to monitor the atmo-
5  sphere and surface. Thanks to their strategic importance these satellites have been, and still are being replaced at the end of their mission. Several cloud CDRs have made use of the long-term data continuity from these satellites, and together they have greatly enhanced our understanding of climate. There are several satellite CDRs based on more than 30 years worth of passive measurements including International Satellite Cloud Climatology Project (ISCCP) (Young et al., 2018), Pathfinder Atmospheres- Extended (PATMOS-x) (Heidinger et al., 2014), Satellite Application Facility on Climate Monitoring (CM SAF)
10  cLoud, Albedo and RAdiation dataset (CLARA)-A2 (Karlsson et al., 2017), and the CDR this paper concerns, Cloud_cci Advanced Very High Resolution Radiometer (AVHRR)-PM v2.0 (Stengel et al., 2017).

All these long-term CDRs have very good spatial coverage and are sufficiently long to capture naturally occurring inter-annual cycles such as El Niño Southern Oscillation (ENSO) and to detect potential climate change signals that emerge from the internal variability (noise) inherent to the climate system. They all have their strengths and weaknesses. For example,
15  ISCCP is well suited for assessing the diurnal cycle of clouds because it uses measurements from geostationary satellites. The other aforementioned data records make use of the spectrally more resolved information from the polar orbiting AVHRR instrument, allowing the retrieval of a wider range of cloud products with presumably higher accuracy.

The Cloud_cci CDR (except its cloud mask and phase identification) has been retrieved using the Optimal Estimation (OE) technique. All cloud properties are radiatively consistent with each other since they were retrieved simultaneously using
20  Visible (VIS) and thermal Infrared (IR) channel measurements. One general benefit to the OE technique is that uncertainties in a-priori estimates and other input data will be propagated and therefore uncertainty estimates are also retrieved together with the solution. The uncertainty retrievals, which provide the modelled random error in the retrieval, are useful since they provide a guide in identifying the CDR's strengths and weaknesses. However, a user still needs to be mindful of systematic errors in retrievals (biases), which are not reported despite often being the most serious source of retrieval error. Systematic
25  errors in retrievals are often heavily situation dependent and can only be estimated by validation against bias-free reference observations.

Other CDRs from passive imagers, such as MODerate resolution Imaging Spectroradiometer (MODIS), Advanced Along-Track Scanning Radiometer (AATSR), Multiangle Imaging SpectroRadiometer (MISR), also provide global cloud products but these satellites are research missions and are not expected to be replaced and have not been around for as long as the
30  AVHRR-based CDRs, so the corresponding data records are shorter and therefore less suitable for climate studies. However, these CDRs are also very valuable since they are based on retrievals from more advanced instruments which measure at more wavelengths, and therefore generally can provide arguably even better cloud retrievals.

Since 2006, climate model developers have made great use of measurements from the satellite-borne active instruments Cloud-Aerosol Lidar with Orthogonal Polarisation (CALIOP) (Winker et al., 2009) and CloudSat (Stephens et al., 2002). These
35  measure the vertical distribution of clouds and the lidar has a much stronger sensitivity to thin clouds than measurements from (nadir-looking) passive instruments, such as those mentioned earlier. The CDRs from these active instruments have immensely

improved our understanding of the vertical structure of clouds and their occurrence in general. They have also been used to constrain the vertical distribution of clouds and their impact on the radiation budget in models. CALIOP and CloudSat data have also served as very accurate references for validating and improving passive imager based cloud retrievals (e.g., Stengel

5   et al., 2015; Karlsson and Håkansson, 2018).

When these CDRs are used for the evaluation of (climate) models, it is important to realise that, in general modelled clouds cannot be directly compared to satellite derived CDRs. In the models, clouds are represented as bulk properties on grids ranging from on the order of $10\,\mathrm{km}$ for regional models to $100\,\mathrm{km}$ for global models, while the observations are made by instruments that typically measure at much smaller scales. The sensitivity of satellite retrievals to clouds also strongly depends on the

10  wavelength at which the measurements are being made as well as the type of cloud that is being observed (Waliser et al., 2009). On top of this, clouds are represented on a three-dimensional spatial grid in models, whereas retrievals based on passive VIS and IR instruments, like the Cloud_cci CDR, do not yield vertically resolved information on clouds, but rather cloud-top and column-integrated cloud properties. Therefore, to assess modelled cloudiness against observations, these and more factors should be taken into account in order to make the modelled and satellite-retrieved clouds comparable.

15  This notion led to the development of so-called satellite simulators. Jakob and Klein (1999) described the first satellite product simulator for the ISCCP CDR. The use of the ISCCP simulator was demonstrated in a model evaluation in Webb et al. (2001). Since then several studies using the ISCCP simulator were made in an effort to constrain modelled clouds, and good progress was made (e.g., Norris et al., 2016; Terai et al., 2016; Tan et al., 2017).

Following the initial developments for ISCCP, many other cloud property- satellite simulators have been established for

20  a range of instruments. Simulators for passive VIS-IR imagers include the MODIS simulator by Pincus et al. (2012) and Spinning Enhanced Visible Infra-Red Imager (SEVIRI) simulators by Bugliaro et al. (2011) and Jonkheid et al. (2012) (The latter reference also provides a conceptual framework of cloud simulators in general and their role in model evaluation.) Quickbeam simulates the vertical profile of clouds that would have been measured by the satellite-borne cloud radar CloudSat, if the model atmosphere was the real atmosphere (Haynes et al., 2007). Similarly a simulator of lidar data was developed for

25  comparison with the Calipso CDR as described in Chepfer et al. (2008). The ECSIM tool (Voors et al., 2007) simulates the instruments in the EarthCARE mission, targeting small-scale cloud fields in particular.

A range of these satellite simulators have been gathered into a simulator package called Cloud Feedback Model Intercomparison Project (CFMIP) Observation Simulator Package (COSP) (Bodas-Salcedo et al., 2011; Swales et al., 2018) which is now considered an indispensable tool for assessing the representation of clouds in climate models. Particularly since there are

30  several different flavours of satellite CDR simulators in COSP, a user can use different simulators to address different aspects of a model (Kay et al., 2012; Webb et al., 2017; Song et al., 2017). The COSP is a self-contained software package that requires model input of vertical cloud, temperature and humidity data. COSP can be installed into a model code so that simulated observational data can be generated and saved together with other model fields. However, COSP can also be used "offline" on archived model data. The main advantage of running COSP integrated into the models' own software environment is to avoid storing large volumes of data otherwise needed for running the simulators afterwards. The disadvantage of installing COSP into a model is that, when installed in the model, run-time is considerably increased (Norris et al., 2016).

Here we present the Cloud_cci satellite product simulator that emulates the Cloud_cci CDR so that climate modellers can make full use of this new CDR and its advantages. This simulator is not yet a part of COSP, but will be included in a branch on the COSP github (https://github.com/CFMIP/COSPv2.0) so that anyone who downloads this publicly available package will automatically have access to this simulator. The usefulness of the Cloud_cci simulator is demonstrated by applying it for an evaluation of the Global Climate Model (GCM) EC-Earth (Hazeleger et al., 2010) and the Regional Climate Model (RCM) RACMO (van Meijgaard et al., 2012).

The structure of this paper is as follows: the EC-Earth and RACMO models are described in Sect. 2.1 and Sect. 2.2, respectively, while the satellite Cloud_cci CDR is outlined in Sect. 2.3. The simulator proposed in this paper is presented in detail in Sect. 3. Results from applying the satellite simulator to EC-Earth and RACMO are given in Sect. 4 and Sect. 5, respectively. Finally, the results are summarized in Sect. 6.

## 2 Models and CDRs

### 2.1 Global climate model: EC-Earth

EC-Earth is a global climate system model. Its atmospheric part is based on the Integrated Forecast System (IFS) of the European Centre for Medium-range Weather Forecasts (ECMWF) model. The version used in this study, EC-Earth3.2beta (Boussetta et al., 2016), is based on IFS cy36r4 in addition to a few important physical adjustments mainly related to the non-orographic gravity wave drag parameterization (latitudinal and resolution dependency of the launch momentum flux) and the diurnal cycle of convection (Bechtold et al., 2014).

To reproduce present day climate variability, EC-Earth was run with prescribed observed Sea Surface Temperature (SST) and sea-ice using European Re-Analysis (ERA)-Interim monthly data as the lower boundary condition, according to the Atmospheric Model Inter-comparison Project (AMIP) protocol. EC-Earth was run with a horizontal resolution of $70\,km$ and on 91 vertical levels. The simulator will be installed in EC-Earth by including the simulator in COSP, but for this experiment the full model vertical fields were stored every 6 hours and the model parameterization formulas for cloud overlap and particle effective radius were used to reproduce the in-model variables needed for the simulator.

The satellite simulated cloud variables were compared with the Cloud_cci AVHRR-PM L3C data record, described in Sect. 2.3 after being aggregated to match the model resolution.

### 2.2 Regional climate model: RACMO

The hydrostatic RCM RACMO2 (van Meijgaard et al., 2012) was originally built from the parameterization package of physical processes employed in the ECMWF Integrated Forecast System (IFS) model merged with the dynamical kernel of the High Resolution Limited Area Model (HIRLAM) (Unden et al., 2002) Numerical Weather Prediction (NWP) model. RACMO2.3 is used in this study. It is based on ECMWF IFS cy33r2, which constitutes large overlaps with the ECMWF physics of cy36r4 used in EC-Earth3.2 as described in Sect. 2.1.

Other physics components include a Turbulence Kinetic Energy (TKE) driven eddy-diffusivity mass-flux scheme (Siebesma et al., 2007; Lenderink and Holtslag, 2004) for mixing and cloud processes in the boundary layer, a scheme for deep convection

5 (originated by Tiedtke, 1989), a prognostic cloud scheme (Tiedtke, 1993; Tompkins et al., 2007), and the land surface/soil scheme Hydrology Tiled ECMWF Scheme for Surface Exchanges over Land (TESSEL) (HTESSEL) (Balsamo et al., 2009). A Rapid Radiation Transfer Module (RRTM) accounts for solar (Clough et al., 2005) and terrestrial radiation (Mlawer et al., 1997). The effect of clouds on radiation at the sub-grid scale is represented by the independent column approximation (ICA; (Morcrette et al., 2008).

10 In the past years, RACMO has been frequently used in transient climate simulations with different GCM drivers (EC-Earth, Hadley Centre Global Environmental Model (HadGEM)2-ES) in the framework of Coordinated Regional Climate Downscaling Experiment (CORDEX) (Giorgi and Gutowski, 2015) and in preparation of the KNMI'14 climate scenarios for the Netherlands (van den Hurk et al., 2014).

For this study, integrations with RACMO were carried out for the years 2011 to 2014 at a 25 km horizontal resolution and

15 40 model levels using a hybrid vertical coordinate. The model domain, configured by employing a rotated pole coordinate, roughly encompasses the region between 30°W to 50°E, and between 30°N and 70°N. The integrations were driven by ERA-Interim atmospheric fields at the lateral boundaries and temperature and sea-ice extent at the sea surface. They were carried out in hindcast mode (instead of climate mode) implying short-term runs of 36 hours. In the chosen set up, runs were re-initialized daily at 12 Coordinated Universal Time (UTC) from ERA-Interim including the land surface state.

20 To avoid effects from spin up, in particular in the cloud fields, the first 12 hours of each run were not considered in the further processing. In this way a quasi-continuous long-term time series of non-overlapping model output was constructed. The benefit of employing hindcast mode rather than climate mode is that the model atmospheric state stays close to the quasi-observed large-scale flow imposed by ERA-Interim, facilitating the comparison of the simulated cloud parameters with those inferred from satellite observations. Multi-level output, including cloud parameters like instantaneous cloud fraction, cloud liquid water

25 content and cloud ice content was archived in 3-hourly resolved files. The Cloud_cci simulator was then applied to this model output on the native RACMO grid.

Simulated model results were compared with the Cloud_cci CDR (see Sect. 2.3), which was aggregated to 25 km resolution in order to match the model resolution. Observed ice cloud fraction and liquid water cloud fraction was calculated from the number of 0.5 degree pixels indicating ice and liquid water clouds, respectively, in the designated 25 km cell. The aggregation

30 of remaining cloud parameters was carried out accordingly.

## 2.3 The Cloud_cci CDR

For this study we use the Cloud_cci AVHRR-PM v2.0 CDR, which contains cloud properties retrieved from global AVHRR observations from the afternoon satellites of the National Oceanic and Atmospheric Administration (NOAA) Earth Observing System (EOS) mission NOAA-7,9,11,14,16,18,19 (Stengel et al., 2017). Created with the Community Cloud Retrieval for Climate (CC4CL) (Sus et al., 2018; McGarragh et al., 2018) using all 5 spectral bands of AVHRR, the following core cloud properties are contained in the CDR: cloud mask (fraction), cloud phase, CTP, visible cloud optical depth at 550nm ($\tau_c$),

5    cloud particle effective radius ($r_e$), and Cloud Water Path (CWP). Except cloud mask and phase, which were determined separately in an initial step, the mentioned cloud properties were retrieved simultaneously applying the OE technique (e.g., Rodgers, 2009). Using these pixels level retrievals, the data was processed to 1) daily composites (Level-3U) which contains un-averaged pixel retrievals sampled onto a global $0.05° \times 0.05°$ latitude longitude grid and 2) monthly mean and histogram products (Level-3C) for which all pixel-level retrievals are averaged (aggregated in case of histograms) within a month on a

10    $0.5° \times 0.5°$ latitude–longitude grid. In this study we used the following data of the Cloud_cci AVHRR-PM v2.0 CDR:

- Global, Level-3C monthly mean products for the period 1982-2014. This data is used for comparisons to global EC-Earth data.

- Level-3U data for a European subset for the period 2011-2014. This data is used for comparisons to RACMO.

Cloud_cci CDR v2.0 has been used in the past for evaluating model data, e.g. (Lauer et al., 2017; Keller et al., 2017; Baró

15    et al., 2018; Lohmann and Neubauer, 2018) although with the limitation of not having the Cloud_cci simulator applied. There are some natural limitations of the Cloud_cci CDR related to cloud sensitivity. For instance the dataset will not contain all thin clouds as they are sometimes too thin to be distinguished by measurements from the AVHRR instruments. Karlsson and Håkansson (2018) found that for the CLARA dataset, which is also based on AVHRR, the global average $\tau_c$ detection limit was $\tau_c$=0.225. Results using the same methods used in the aforementioned paper found a slightly lower global limit at $\tau_c$=0.2

20    (0.21) for version 2 of the Cloud_cci CDR (Karlsson and Devasthale, 2018). This limit is however not to be understood that all clouds with smaller $\tau_c$s are missed, rather then the occurrence of clouds with smaller COTs is underestimated. The threshold further represents a global mean value; the sensitivity to thin clouds often depend on, for example, illumination conditions as well as surface type and temperature.

Measurements from AVHRR used in the Cloud_cci CDR do in most cases not provide enough information to distinguish

25    multi-layer from single-layer clouds, and this can lead to large uncertainties in the derived cloud retrievals. If an opaque cloud is overlapping any cloud, the cloud top properties will belong to the upper cloud. However, if a low cloud is overlain by a semi-transparent high cloud, the measured upwelling radiation will contain information from both cloud layers, and potentially the underlying surface and the cloud top properties cannot be correctly retrieved. Such cases may be misclassified as mid-level clouds adding uncertainty to the cloud retrievals, especially retrievals of mid-layer clouds. Also the low cloud fraction may be

30    underestimated due to overlapping high clouds obscuring them from satellite view. One task of the developed simulator is to account for this limitation in the observations.

## 3    Cloud_cci simulator

The Cloud_cci simulator has been developed to enable modellers to compare model cloud fields to the Cloud_cci CDR. Within the Cloud_cci project, a simplified simulator called SIMplistic cloud simulator For ERA-interim (SIMFERA) was developed (Stengel et al., 2018) aiming at comparisons with model reanalysis datasets such as ERA Interim in offline mode. The main difference between SIMFERA and the simulator introduced here is that it mainly tackles the discrepancies in horizontal and

Geoscientific
Model Development
Discussions

5   vertical scales between the observations and model with minimal modifications to the basic model output. The Cloud_cci simulator presented here follows closely the methodology of the other simulators for passive sensors in COSP, especially the MODIS simulator. As with the other simulators in COSP, this simulator requires grid averages on model levels as input for cloud cover, cloud water content, cloud effective radius and temperature.

  The first step in the simulator is downscaling the horizontally relatively coarse model grid boxes to the resolution of the 10  satellite data. For this purpose the sub-sampler as described in Jakob and Klein (1999) and as included in COSP is used. The sub-sampler creates sub-grids within the native model grid and maps the model layer cloud fractions onto the sub-columns in a manner consistent with the cloud overlap assumptions made in the model. Both EC-Earth and RACMO employ the maximum–random overlap assumption, which, in short means that vertically adjacent clouds are treated as maximally overlapping while vertically separated cloud layers are assumed to have random overlap. This information is lost from the grid averaged modelled 15  fields, but is necessary to replicate in the simulator for a fair comparison.

  In-cloud $\tau_c$ is calculated for each model layer and separately for ice and liquid from in-cloud water contents and $r_e$, after which these properties are copied from the model grid to the cloudy levels of the sub-columns. The simulated $\tau_c$ is the integral sum of the partial optical depths ,$\tau_i$ in the sub column. After this step, the simulator mimics the Cloud_cci CDR cloud mask by treating all sub-columns with an integrated cloud optical depth less than the limit for "thin clouds" ($\tau_c < 0.2$, see Sect. 2.3) 20  as cloud free, and the rest as cloudy. The simulated average $\tau_c$ is simply the linear average $\bar{\tau}_c(\tau_c > 0.2)$ per grid box. Both linear and log averaged $\tau_c$ are available variables in the Cloud_cci CDR, and here the simulated $\tau_c$ corresponds to the linearly averaged $\tau_c$.

  The cloud fraction is simulated by counting the number of cloudy sub-columns divided by the total number of sub-columns per grid. Cloud fractions are also provided for low (CTP $> 680\,$hPa), mid ( $680\,$hPa$<$ CTP $<440\,$hPa), and high (CTP 25  $<440\,$hPa) clouds so that the user may focus on these cloud categories separately.

  The cloud phase is "retrieved" in nearly the same manner as done by the MODIS simulator described in Pincus et al. (2012). The cloud phase is determined from the highest-most cloudy region in the sub-columns between the Top of Atmosphere (TOA) to one optical depth down into the cloud according to:

$$p = \mathrm{NINT} \left( \frac{\sum_{\mathrm{TOA}}^{\tau} \tau_i^{\mathrm{liq}} + 2\tau_i^{\mathrm{ice}}}{\sum_{\mathrm{TOA}}^{\tau} \tau_i^{\mathrm{liq}} + \tau_i^{\mathrm{ice}}} \right) \tag{1}$$

30   where $\tau = \min(1, \tau_c)$ and where $\tau_i^{\mathrm{liq/ice}}$ are the partial optical depths for liquid and ice phase respectively in a model layer, $i$. NINT means "the nearest integer". As can be deduced from 1, if the top of the cloud is mostly ice ($p$=2), the phase is retrieved as such, and vice versa for liquid ($p$=1). Note also that all cloudy columns are determined to be one phase or another, hence never undetermined.

Geoscientific
Model Development
Discussions

**Table 1.** The cloud variables produced by the simulator. The middle column specifies the separate categories available for each variable, and the third column indicates under which illumination conditions the variables are available

| Cloud variable | Categories | day/night |
|---|---|---|
| Cloud fraction | total, ice, liquid, low, mid and high | day and night |
| Cloud top | height, temperature, pressure | day and night |
| $\tau_c$ | liquid, ice | day only |
| $r_e$ | liquid, ice | day only |
| CWP | liquid, ice | day only |
| CTP-$\tau_c$ 2D histograms | liquid, ice | day only |
| Cloud albedo | | day only |

The CTP is found at the model pressure ($P$) where $\tau_c$ reaches $\tau_c = 1$ integrated from the TOA, or in the case when $0.2 < \tau_c < 1$, the cloudy model level closest to the surface:

$$\text{CTP} = P\left(\tau = \min(1, \tau_c)\right) \tag{2}$$

In this way the simulator emulates the difficulty in retrieving multilayered clouds. Cloud Top Height (CTH) and Cloud Top Temperature (CTT) are set to the model height and temperature, respectively at the same level where CTP is simulated. The grid average CTP is calculated by log-linear averaging of the sub-grid CTPs, as opposed to linear averaging for all other simulated grid averages. The $r_e$ is also simulated using the same approach as the MODIS simulator, i.e. performing a simplified pseudo-inversion as described in Pincus et al. (2012). However, the simulated Cloud_cci differs from MODIS since, for consistency with the Cloud_cci CDR, the simulator uses the same cloud particle models as used in Cloud_cci retrievals (McGarragh et al., 2018), and they differ from those used in the MODIS retrievals. Liquid Water Path (LWP) and Ice Water Path (IWP) are calculated from the simulated $\tau_c$ and $r_e$ in the same manner as for the Cloud_cci CDR which follows Stephens (1978). The cloud albedo is derived from LUTs as a function of simulated $r_e$ and $\tau_c$, and the solar zenith angle.

The simulator makes use of a solar zenith angle limit ($\Theta_0 < 80°$) to ensure that retrievals which can only be made during daytime conditions are only simulated during daylight hours. See Table 1 for a complete list of the variables simulated by the Cloud_cci simulator.

## 3.1 The impact of using a simulator on cloudiness

To demonstrate the importance of using satellite simulators for model to observation comparisons of cloud variables, we assess the separate impact of 1) sampling the model to match the satellite overpass times and 2) the impact of taking into account the under-representations of very thin clouds in the dataset due to limited satellite sensor sensitivities. These two aspects influence the simulations to a different extent depending on the variable. First we demonstrate the consequence of diurnal sampling on LWP, one of the variables expected to be strongly impacted by the diurnal cycle.

### 3.1.1 Temporal sampling

5    To not take the temporal sampling of the satellites into account is a potentially strong error source in model to satellite comparisons for certain cloud variables such as cloud water, with the uncertainty increasing with increasing model resolution (Guan et al., 2013). So far it is the responsibility of the user to ensure that the temporal sampling of the model matches that of the satellite, and many publications, such as in Ban-Weiss et al. (2014) rightly take the Equatorial overpass time (EOT) into account when doing model comparisons. However, if a user compares simulated output from the model directly to observations

10   without taking into account the EOT of the satellites used to make the CDR, bias due to temporal sampling will be introduced. Fig. 1 shows the EOT of the satellites used to make the AVHRR-PM version of the Cloud_cci CDR.
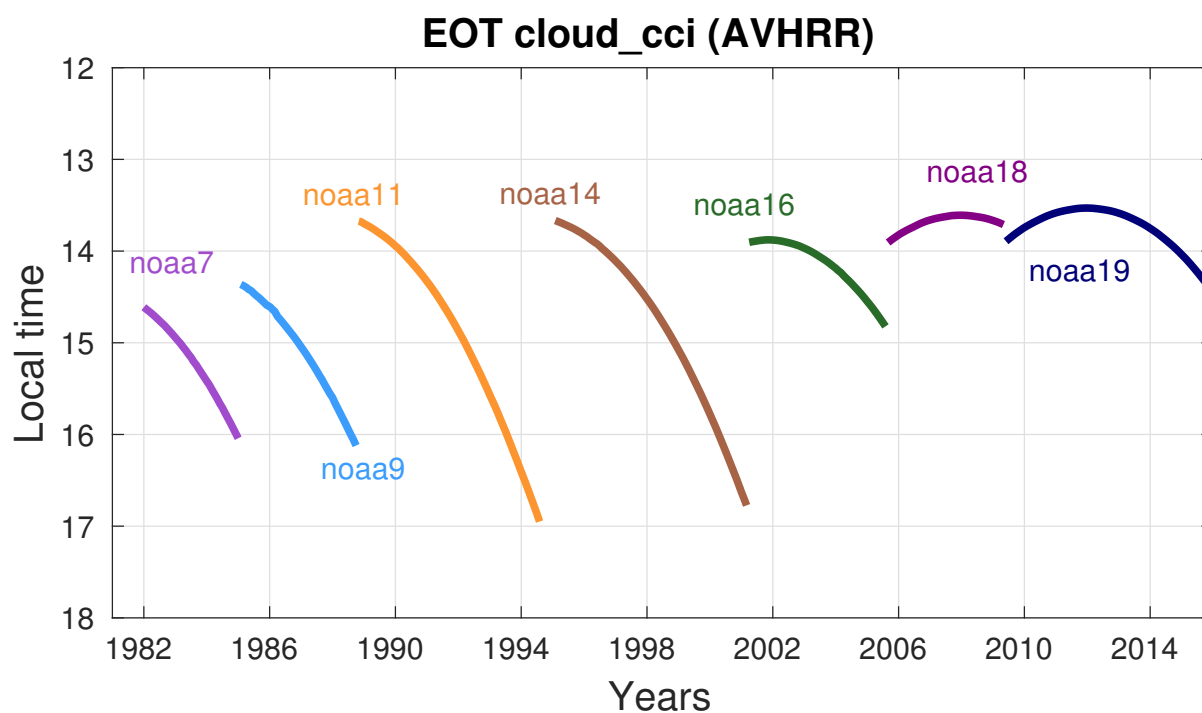
**Figure 1.** The local time of EOT of the daytime (ascending) nodes of the satellites used to create the Cloud_cci AVHRR-PM CDR. The figure is a modified version of the same data in Stengel et al. (2017)
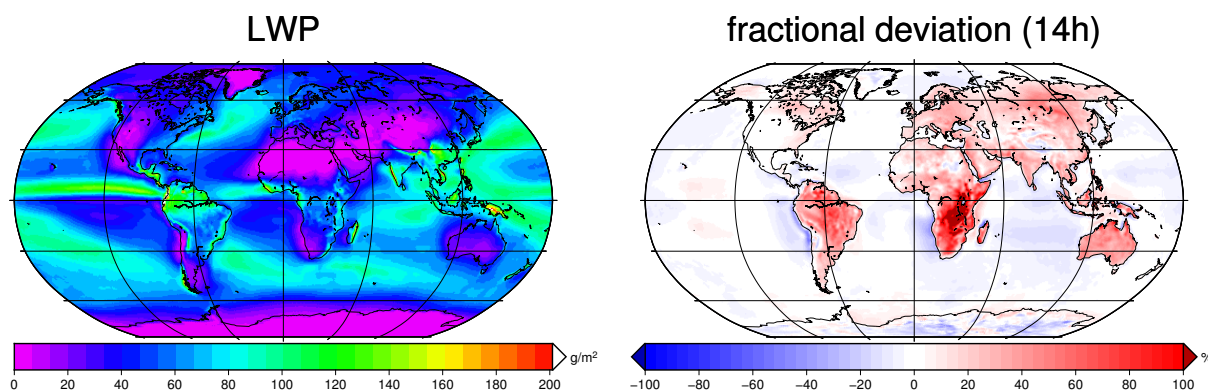
**Figure 2.** The total average LWP from EC Earth based on available all time steps (left), and the fractional deviation of the average LWP from sampling at 14:00 local time compared to the day average ($100 \times (\frac{\text{LWP}_{14}}{\text{LWP}_{\text{ref}}} - 1)$). The data are directly from the model from the period 1982 to 2014.

These polar orbiting satellites start sampling the Earth at mid-afternoon[1] globally at the start of their lifetime, but the local time of sampling "drifts" slowly over time if a satellite does not actively compensate for this. For instance, at the start of the period when the Cloud_cci CDR is based on NOAA-11 (November 1988), the EOT is around 13:30 local time, and just
15 before switching data source to NOAA-14 (February 1995), the EOT is close to 17:00 local time. Especially in areas where the diurnal cycle of clouds or their properties is strong, the effect of sampling the atmosphere at later and later local times may be misinterpreted as cloud trend.

The impact of not taking the satellite overpass into account is demonstrated in Fig. 2 using the original model data (i.e., not simulations of Cloud_cci) of LWP, one of the variables impacted the hardest by temporal sampling (Guan et al., 2013). The
20 average LWP is on the left, and the fractional deviation between the average LWP at 14:00 and the total day average is on the right. 14:00 is the local time chosen for comparison here since it is near the nominal EOT of the ascending node of the afternoon satellites using this version of the Cloud_cci CDR (see Fig. 1).

As can be seen in Fig. 2, the largest biases can be between around $50\%$ to $100\%$ when comparing the average at 14:00 local time to the average from all the model data. The biases at this local time are largely positive over land, and negative (and
5 smaller) over ocean at this sampling time. The bias is most prominent over tropical land, which tends to be more cloud free in the morning while very often thunderstorms develop in the afternoon, and in the oceanic regions off the west coasts of the continents where conditions are dominated by stratocumulus in the morning which mostly clears up during the day.

As can be seen in Fig. 1, there are periods in the CDR where the sampling EOT is far off 14:00. For instance for the periods near the end of NOAA-7 and NOAA-9, and longer periods near the end of NOAA-11 and NOAA-14 data series the EOT is 16:00 or later. At 17:00, the extreme, the bias pattern is quite different with large areas of negative and positive differences compared to the day-mean (not shown).

---

[1]This is as the satellite ascends from south to north, the descending EOT is shifted 12 hours from the ascending node
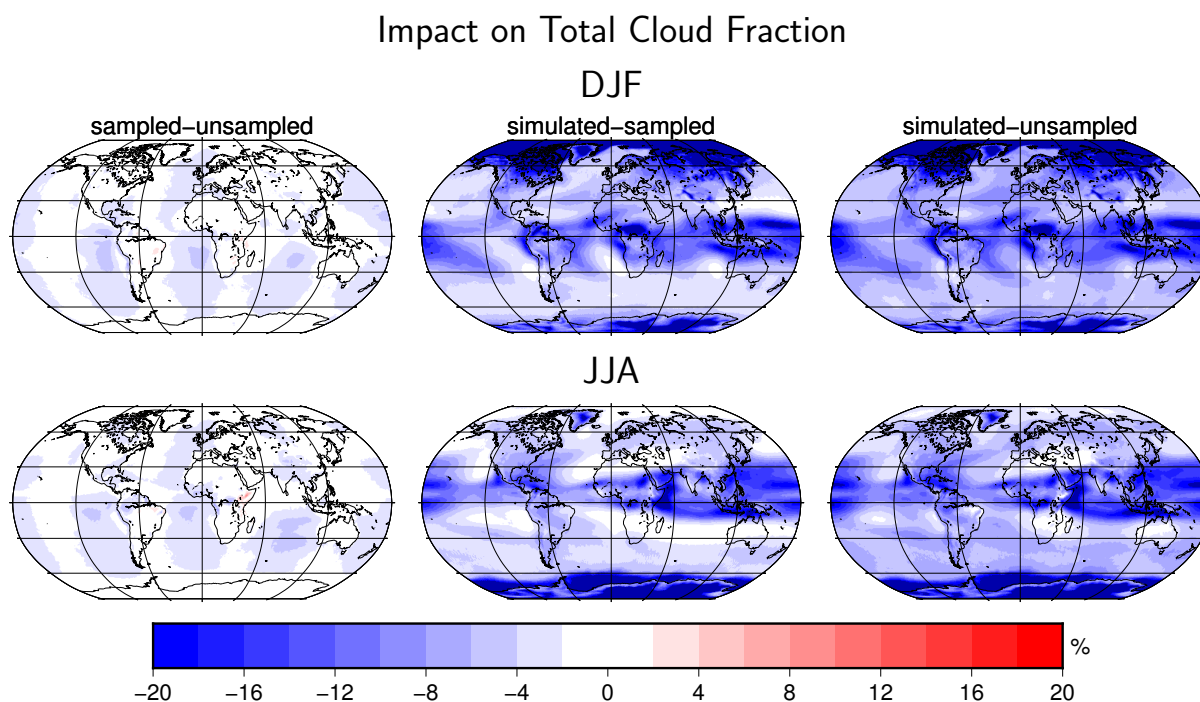
**Figure 3.** The simulated TCF minus the model TCF. The leftmost column shows the impact of sampling the model to match the EOT of the satellites in a similar way as in Fig. 2, but this time for TCF and using the EOT shown in Fig. 1 (sampled model minus unsampled model), the middle column shows the simulated lack of sensitivity of the AVHRR sensor to optically very thin clouds ($\tau_c < 0.2$) (simulated Cloud_cci - sampled model), and the rightmost column shows the combined impact on these two effects (simulated Cloud_cci - unsampled model). The top row is valid for December, January, and February (DJF), and the bottom is for June, July, and August (JJA). The data covers the period 1982–2014.

In general, the geographic regions where there is a strong diurnal cycle are expected to be where the largest sampling errors will occur. We decided for the sake of reducing the temporal sampling bias the Cloud_cci simulator should include the satellite 5 overpass times as a function of year, month, and satellite so that the model can be automatically sampled at the local time that best matches the satellite and time period.

### 3.1.2 Cloud sensitivity

Using the basic cloud variable TCF, we demonstrate the combined effect of temporal sampling and removing clouds too thin to be retrieved in the Cloud_cci CDR. Fig. 3 shows separately these two important effects of the simulator: sampling the data 10 at the correct satellite overpass time as described in the previous section (left), removing clouds too thin to be retrieved in Cloud_cci (centre), and their combined effect which is the translation from model TCF into simulated TCF (right).

Overall, the simulator clearly reduces the TCF. The left column of Fig. 3 showing the difference between sampled and unsampled model data, illustrates that the effect of temporal sampling is important but nonetheless not as important as the effect of removing all thin clouds (center column) to the total difference between the simulated cloud_cci and the unsampled model. There are two important features to mention about the sampled minus unsampled difference; Unlike LWP, TCF is retrieved both during daytime and nighttime and therefore TCF is the average from 2 satellite overpasses per day, mostly around 2PM and 2AM local time (see Fig. 1), as opposed to LWP retrievals which can only be retrieved during daylight hours (2PM). Therefore the error introduced by not sampling the model data is less for day-and night variables such as TCF compared to daylight only variables.

Another feature is a clear interference pattern that is seen in the difference between the sampled and the unsampled model data. The longitudinal interference pattern appears at $90 \, \mathrm{degree}$ intervals where the difference between the sampled and unsampled data reduces to exactly 0. This is a side effect from linearly interpolating between model time steps in order to sample the model data at a common local time that matches the EOT of the satellite. At evenly spaced longitudes, sampling the model to the ascending and descending EOT is found from, for example, data at exactly $0.5 \times 6 \, \mathrm{UTC} + 0.5 \times 12 \, \mathrm{UTC}$ for the ascending node and $0.5 \times 18 \, \mathrm{UTC} + 0.5 \times 24 \, \mathrm{UTC}$ for the descending node. The average of these two interpolated values here is exactly the same as the average of the 4 model times steps at this longitude. This leads to a pattern of minimum and maximum differences that is repeated $\frac{360°}{N}$ times, where $N$ is the number of model times steps per day. The longitudes at which the minima are found depend on the EOT of the satellite. The interference patterns are a little blurred since the EOT is not constant over 33 years. This effect should also be present on top of any 'real' differences whenever observational data based on two satellite overpasses per day is compared to model data when no attempt at temporal sampling has been made.

The global mean TCF is reduced by the simulator by about $10\,\%$. As a reference, using CALIOP v4.0 data, we established that a global average of about $14\,\%$ are "thin clouds" ($\tau_c < 0.2$). Noteworthy from Fig. 3, the TCF is reduced by up to $20\,\%$ in some regions such as in large swathes of the Tropics and Polar regions, whereas for others such as at mid-latitudes TCF is only lightly impacted. This can be explained by the model correctly reflecting the observed high frequency of thin Cirrus clouds in the Tropical regions (Sassen et al., 2008) which are re-classified as cloud free by the simulator. In the Polar regions, EC-Earth tends to have a high frequency of very thin, and likely false clouds which are also removed by the simulator. The regional distribution of the effect of the simulator on TCF is quite different depending on the season. The impact on TCF by the simulator over South-East Africa in JJA is an increase in cloudiness because the temporal sampling effect described in Sect. 3.1.1 has a positive sign and is larger than the reduction by removing thin clouds..

## 4 Results EC-Earth

### 4.1 Cloud fraction

Several studies have made use of the layered cloud cover for assessing the climate variability in GCMs (Zhang et al., 2005). The cloud cover varies quite substantially on a seasonal basis as seen by comparing JJA, Fig. 4, and DJF, Fig. 5. The TCF is included in each figure for reference and is the sum of the low, mid, and high layers.
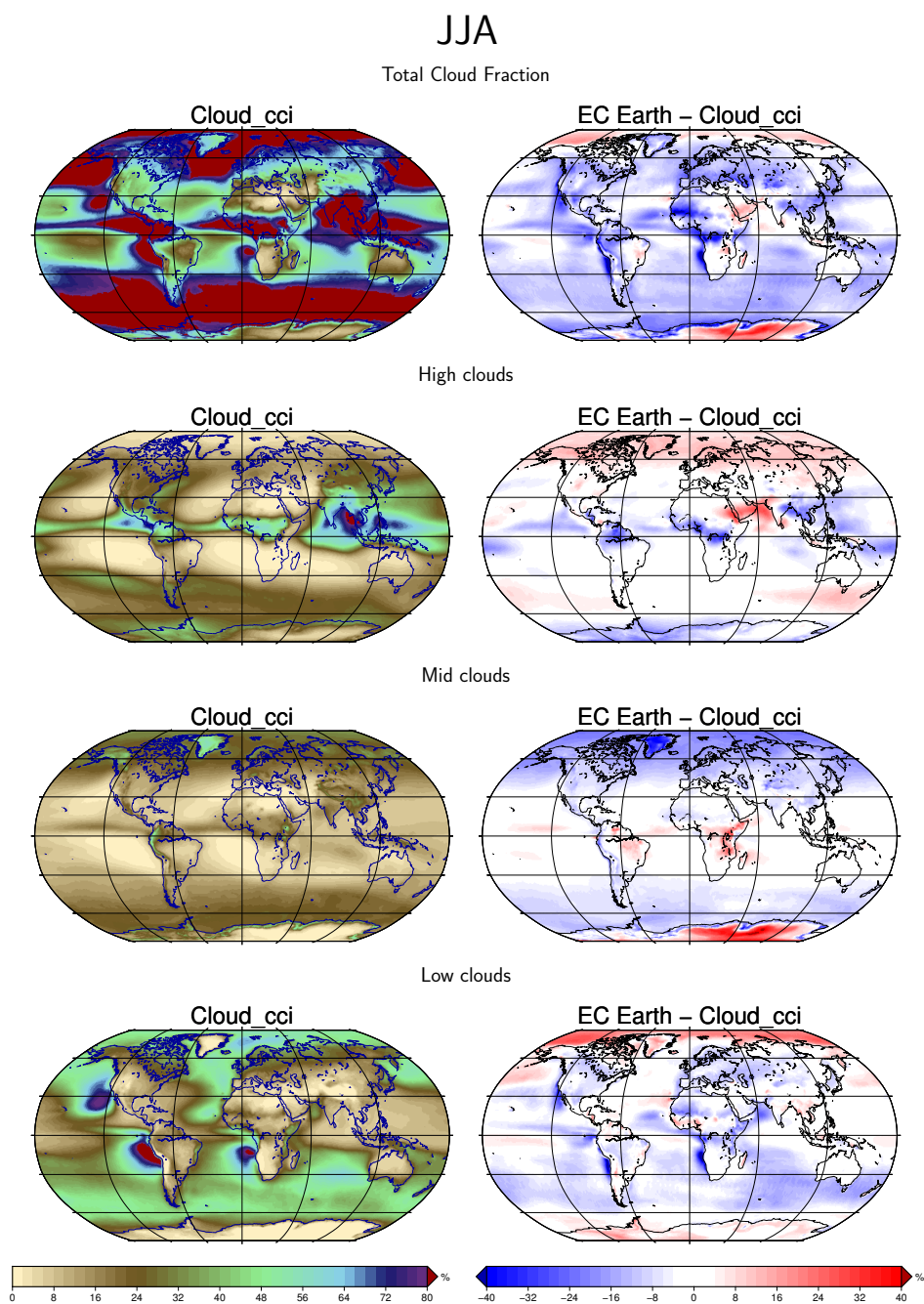
**Figure 4.** Cloud fractions separated by cloud altitude from the Cloud_cci CDR (left column) and difference between the simulated Cloud_cci based EC-Earth atmosphere and the observations (right column), separated into TCF (top row), high clouds (second row), mid-level clouds (third row), and low clouds (bottom row), for JJA.
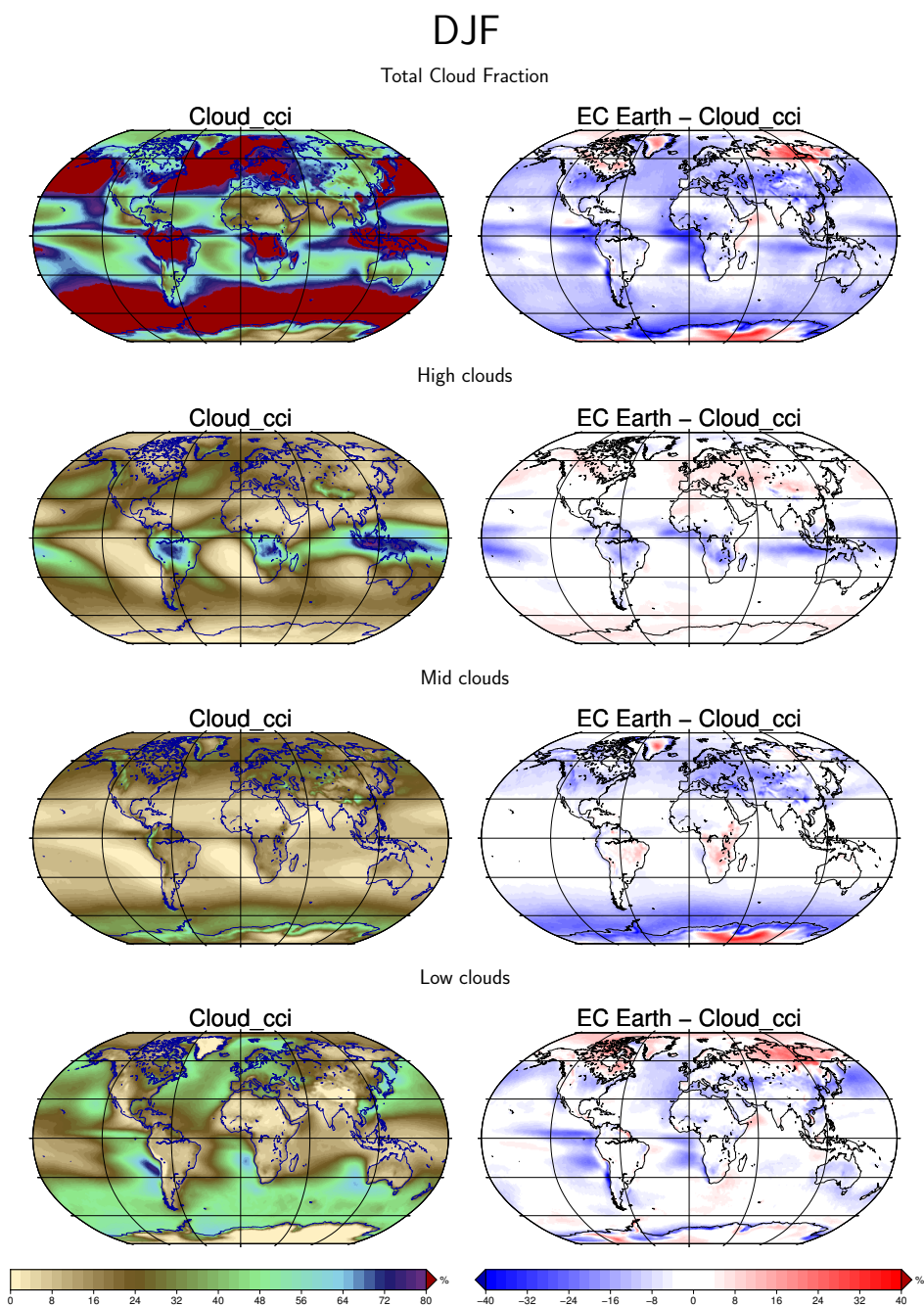
**Figure 5.** Same as Fig. 4, but for DJF.

Overall, the distribution of high clouds is reasonably well captured by EC-Earth, although the simulations show an overall underestimation of tropical high cloud fraction. EC-Earth seems to have too few clouds associated with the Inter-Tropical Convergence Zone (ITCZ) in general in both seasons. Also, it appears the high clouds associated with the Indian Monsoon may be too far west in EC-Earth during JJA as seen by the very large overrepresentation of high clouds over the Arabian subcontinent and sea (around $20\%$ more than the observations). There is a larger deficit of high clouds over Tropical Africa and South America in JJA compared to DJF.

For low clouds, a prominent feature is the large deficit in (or large under-prediction of) cloudiness in the subtropical maritime Stratocumulus regions off the west coast of Southern Africa, South America, and Southern North America especially in JJA but also in DJF. Underestimation of subtropical maritime clouds is common in climate models and is largely due to a lack of regional variability in low cloud fraction in these regions (Noda and Satoh, 2014), which is linked to the variability of atmospheric stability of the lower atmosphere (Sun et al., 2011). Low clouds are under-predicted everywhere except for the polar regions as found previously for EC-Earth (Koenigk et al., 2013).

Outside the Tropics, the model cloudiness may be quite feasible if one takes into account that the Cloud_cci CDR may place some thin high clouds too low in altitude, artificially decreasing the high cloud fraction and increasing the amount of mid-level clouds. However, the strong negative cloud fraction bias in some regions can only be partially explained by this. The negative bias in tropical high clouds could be in part a consequence of the simulator removing too many clouds in these regions, or that the model has them optically too thin. But also, since this simulator like the MODIS, and ISCCP simulators, uses a global constant $\tau_c$ threshold, it may be a little too high for the Tropics, and too low for other regions compared to the actual performance of the Cloud_cci cloud mask of this version of the dataset.
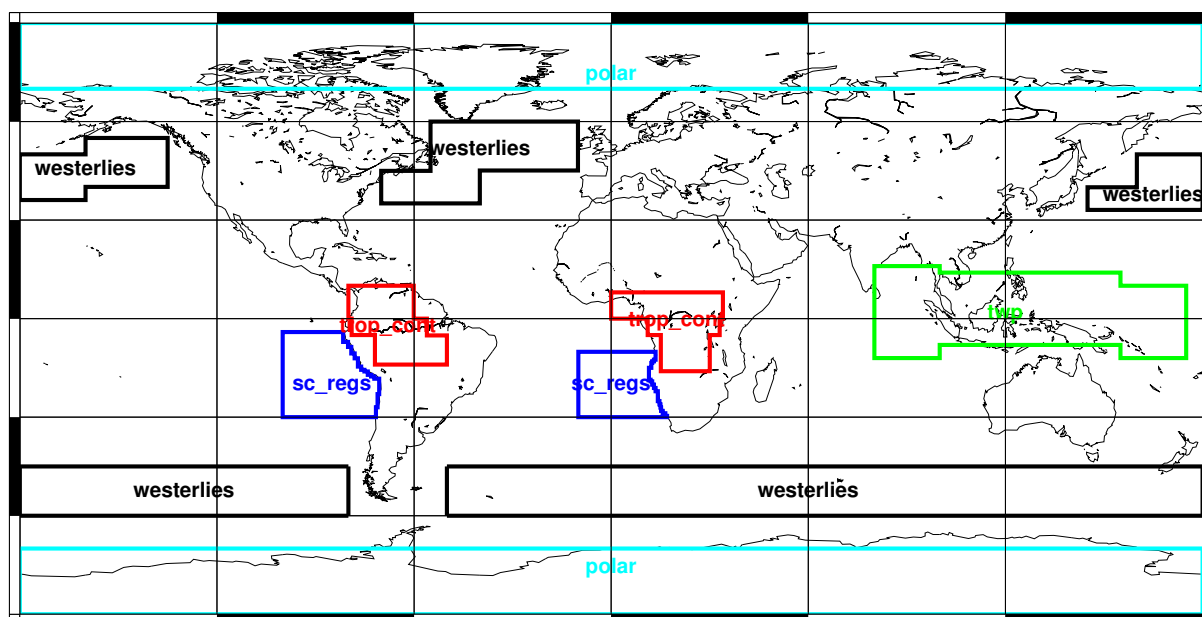
## 4.2 Cloud vertical distribution

**Figure 6.** A map of the regions selected for further investigation adapted from (Eliasson et al., 2011, Fig 9.).
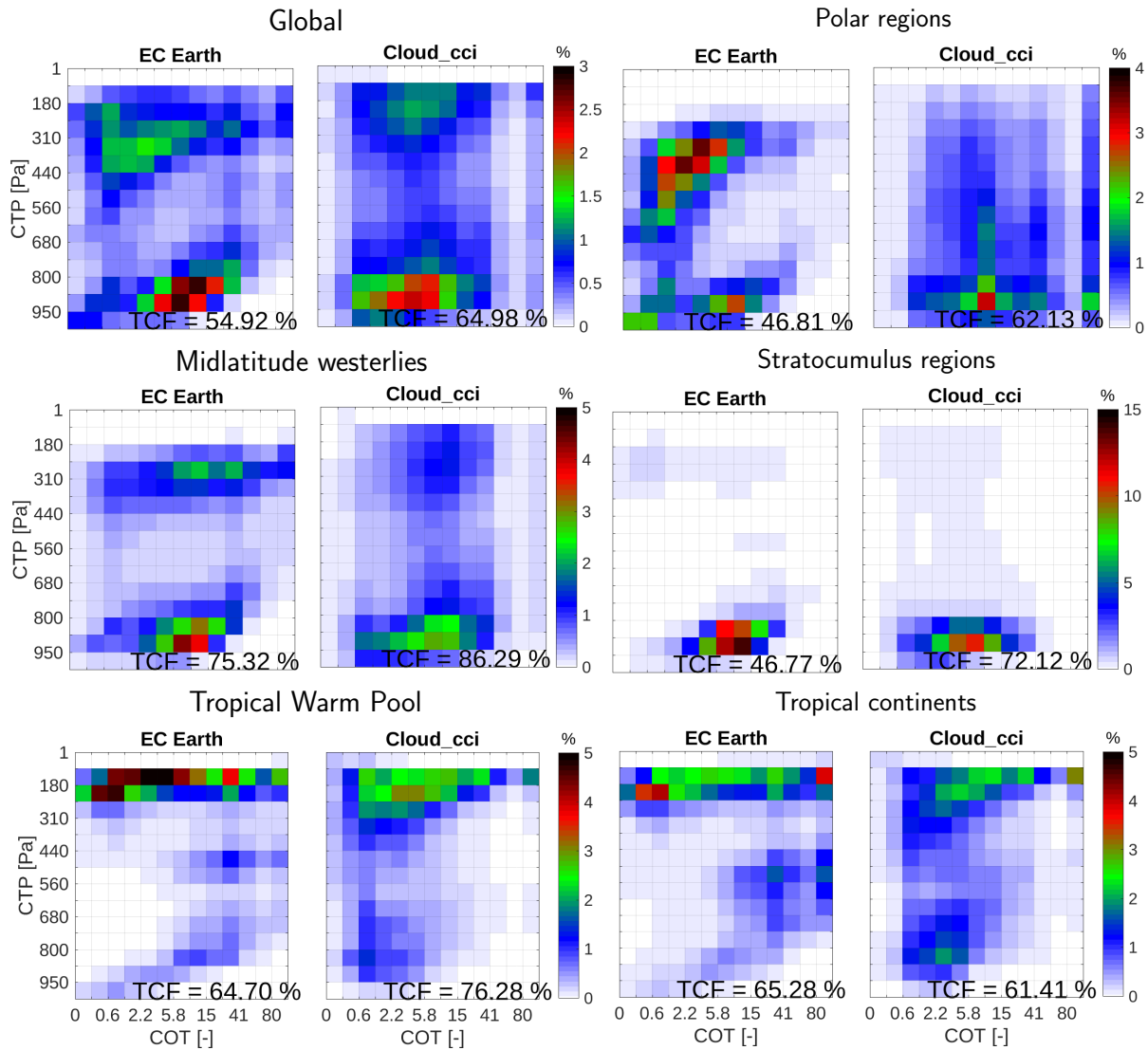
# CTP-$\tau$ 2D histogram



**Figure 7.** CTP–$\tau_c$ histograms of simulated Cloud_cci based on EC-Earth (left) and the Cloud_cci CDR (right) for selected regions (see Fig. 6). Total cloud fractions for each region are indicated in the panels.

By using the CTP-$\tau_c$ histograms shown in Fig. 7, more information on the difference in cloud vertical distribution can be found. Globally EC-Earth is less cloudy than the Cloud_cci CDR by about $8\,\%$. The CTP-$\tau_c$ distribution of clouds is quite different between the model and observations and better understanding of the differences can be found if one separates the distributions into separate climatological regions (Eliasson et al., 2011). Here we focus on five noncontiguous regions shown on the map in Fig. 6.

18

In the Polar regions, the vertical distribution of clouds deviates strongly from the Cloud_cci CDR. EC earth has a high frequency of relatively thin, mid-high clouds, a feature completely missing from the Cloud_cci CDR. However the datasets'

15 skill in the Arctic may be insufficient to make definitive claims about biases in the model. In the Westerlies region there are fewer mid-level clouds in the model than in the observations in general. This difference may be attributed to misclassifications of multi-layer clouds into mid-layer clouds by the Cloud_cci CDR, by the process mentioned in the previous section. The reason EC-Earth has a higher occurrence of high clouds in the Westerlies region may be the same, but there are indications that EC-Earth has too many very optically thick high clouds in the Westerlies regions.

20 In the maritime Stratocumulus regions, the model clearly underestimates the amount of clouds by about $15\,\%$, as well underestimating the diversity, in terms of thickness and vertical distribution, of low clouds compared to the Cloud_cci CDR. In the Tropical Warm Pool (TWP) region EC-Earth is less cloudy, but tends to have substantially thicker clouds. In the tropical continental regions, EC-Earth erroneously has many more mid-level, optically thick clouds and is missing the regular occurrence of low level thin clouds. EC-Earth also has relatively much more high-level thin clouds compared to observations, although it

25 has a lower total cloud fraction. Quite potentially, the mid-level clouds in the model are too thick.

### 4.2.1 Cloud Top Pressure

The mean CTP is shown in Fig. 8. Overall, the cloud top pressure in the midlatitude regions are fairly close to the observations. However, there are other areas with large differences such as the polar regions, where EC-Earth has much higher CTP (lower CTH), but the polar regions are also difficult places for cloud retrievals from any passive instrument, since very cold regions

5 risk having a bias towards lower level clouds as high clouds have similar cloud and surface temperatures. This makes retrievals in these regions quite uncertain. More important are the differences found in the Tropics since clouds there are generally easier to retrieve due to the large temperature contrast between the warm surface and especially mid- and high-level clouds. EC-Earth tends to overestimate the CTP compared to the Cloud_cci CDR around the outskirts of the TWP and especially in the central Pacific, a region where clouds are heavily influenced by the ENSO. In contrast, in a large region covering North Africa and

10 the Arabian subcontinent the clouds in the model appear much higher (lower CTP) compared to the Cloud_cci retrievals. This may be a consequence of too many high clouds as mentioned in the previous section, or the effect of thin high cirrus over the desert (which has a lower surface emissivity) being retrieved as mid-level clouds, or a combination of these reasons.
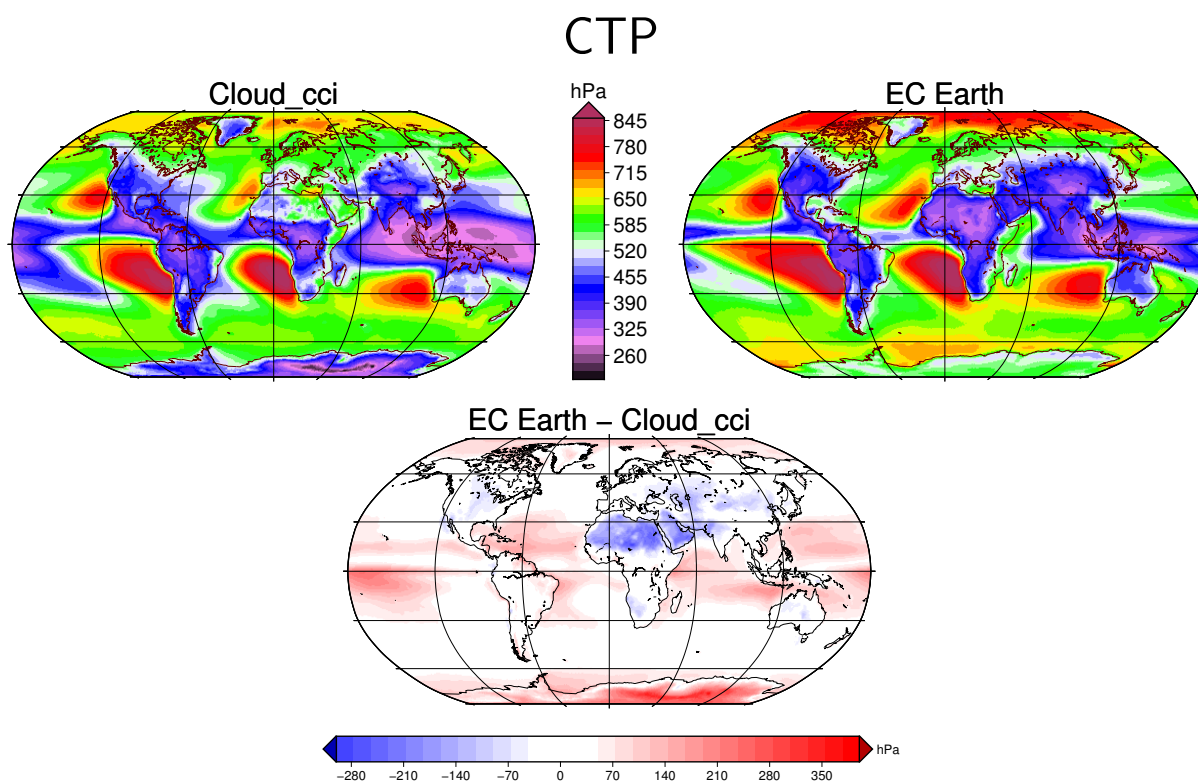
**Figure 8.** The CTP from the Cloud_cci CDR(top left), simulated CTP based on EC-Earth (top right) and the difference between the two (bottom). The data cover the time period 1982-2014.
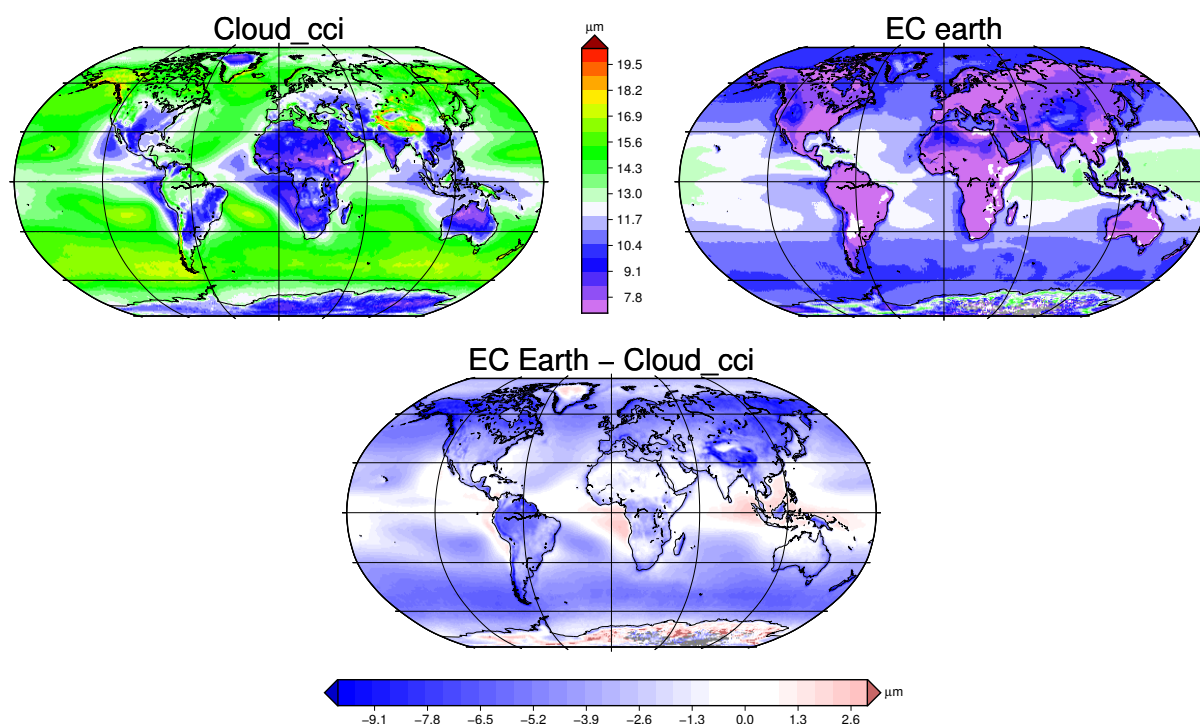
## Cloud liquid effective radius



**Figure 9.** Same as for Fig. 8, but for liquid $r_e$.

### 4.3   Effective radius

Cloud microphysical properties strongly influence the radiative budget and also the water cycle. However, properties such as $r_e$ may be difficult to compare between models and satellite observations since their uncertainties are quite large and depend strongly on the assumptions, such as optical properties of cloud particles, that must be made in the retrieval process.

5        The differences between EC-Earth and the Cloud_cci CDR are substantial. As can be seen in Fig. 9, the differences are very large in terms of liquid cloud $r_e$. There is a very distinct land-sea difference, which is likely a reflection of the model $r_e$ parameterizations based on Martin et al. (1994). These depend in part on the assumed aerosol concentrations, which are largely different over land and sea. EC-Earth assumes one constant concentration of $900\,\mathrm{cm}^{-3}$ over land and $50\,\mathrm{cm}^{-3}$ over sea. However, the differences can also be due to problems of the $r_e$ retrievals, e.g. for broken and multi-layer clouds. There is also a strong disagreement in terms of ice $r_e$ (not shown). The skill of the retrieved ice cloud $r_e$ in v2.0 is questionable according to Stengel et al. (2017), and therefore left out in the comparisons for EC-Earth and RACMO in the next section. Overall, the observations and EC-Earth are in disagreement for $r_e$ and deeper analysis is needed to find the sources to these differences.
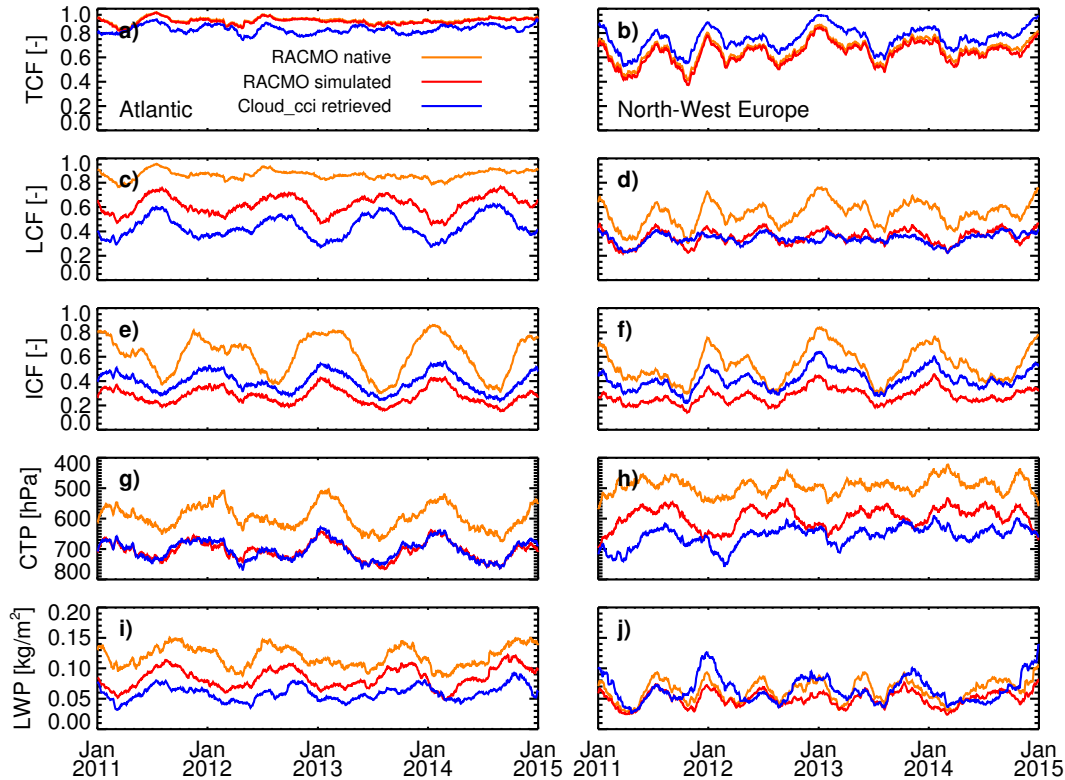
**Figure 10.** Time series of RACMO native model (orange), simulated (red), and Cloud_cci retrieved (blue) cloud properties for areas in the Atlantic (left;25–15 °W, 48–53 °N) and North-West Europe (right; 5–15 °E, 48–53 °N) during 2011–2014: a)+b) total cloud fraction, c)+d) liquid cloud fraction, e)+f) ice cloud fraction, g)+h) CTP (hPa), and i)+j) LWP ($kg\,m^{-2}$). Shown are 2-month running means. All properties are all-sky linear averages, except CTP, which is an in-cloud logarithmic average.

## 5    Results RACMO

This section describes the performance of the RCM, RACMO compared to the Cloud_cci CDR using the satellite simulator. In Fig. 10, time series of RACMO cloud property simulations are compared with the Cloud_cci CDR retrievals for two selected areas: in the Atlantic and in North-West Europe (see Fig. 11a for the location of these areas). For these regions the simulator does not change the RACMO TCF much, i.e. the contribution of thin clouds is very small. Note that this differs somewhat from the EC-Earth run, which has, especially over the Atlantic region, a larger amount of thin clouds and consequently a stronger reduction in TCF induced by the simulator (cf. Fig. 3). Compared to the satellite observations, the model overestimates TCF in the Atlantic, while the opposite is true over North-West Europe.

The cloud fraction is further separated into liquid and ice cloud fractions (LCF/ICF). In the model a grid box can contribute to both cloud fractions, so the sum of LCF and ICF will in general be larger than TCF. In the simulator, as well as in the retrieval, a column is either designated the liquid or the ice phase, so that the two fractions will add up to TCF. As a result, the simulator decreases both LCF and ICF compared to the native model, making it much more comparable to the retrievals. The CTP in the model is much smaller than retrieved, i.e. the cloud tops are higher. The simulator increases log-mean CTP by about $100\,\mathrm{hPa}$ in both regions by removing modelled thin high cloud layers, bringing it much closer to the satellite retrieval. To multi-phase clouds in the model (typically ice above liquid), the simulator will tend to designate the ice phase. The liquid water in the lower clouds is then basically interpreted as ice. Consequently, the simulated LWP is smaller than in the native model. In the Atlantic this leads to a closer agreement with the satellite observations. In North-West Europe the native model LWP is on average already comparable to the satellite measurements, and the simulator turns this into an underestimation.

For the Cloud_cci CDR and the areas shown in Fig. 10, the correlation coefficient (Pearson's $r$) between simulated and retrieved time series ranges between 0.55 (for TCF over the Atlantic) and 0.86 (for TCF in North-West Europe and ICF in both regions). In general, the simulated time series correlate (much) better with the retrievals than the native model time series. As an indication, the mean correlation coefficients for the two regions and five parameters considered are 0.56 and 0.74 for the native-modelled and simulated time series, respectively.

Spatial distributions of modelled and retrieved cloud properties are shown in Fig. 11. As noted before, the simulator has a relatively small impact on RACMO TCF, with a reduction of about $2\,\%$ over the model domain. The modelled and retrieved spatial patterns in TCF correspond rather well. Note for example the agreement in orography-related TCF patterns in the Alps and Carpathians. However, the model (and simulated) TCF is higher than the retrieval over the Atlantic, particularly in the southern part of the domain, where differences reach 20%. The opposite is true over most of the continent, including the Baltic Sea and the Black Sea. An underestimation of RACMO TCF compared with satellite retrievals over the (western) European continent was also found by Roebeling and van Meijgaard (2009).
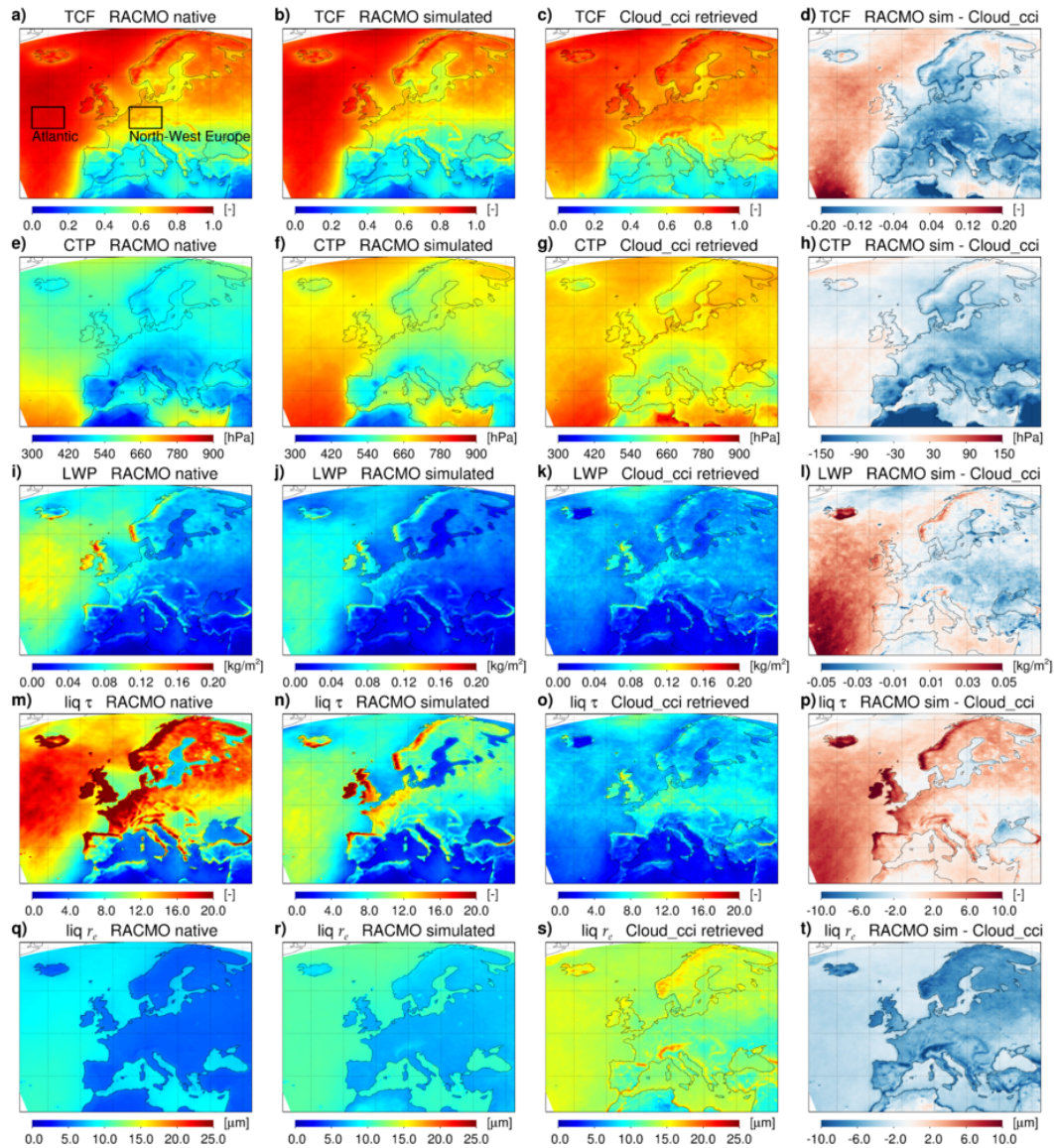
**Figure 11.** Maps of 2011—1014 mean modelled and retrieved cloud properties: a-d) total cloud fraction, e-h) cloud top pressure (hPa), i-l) LWP ($kg\,m^{-2}$), m-p) liquid $\tau_c$, and q-t) liquid cloud droplet effective radius (μm). The columns show from left to right the native model, the simulator, the Cloud_cci data, and the difference between simulator and retrieval. All properties are all-sky averages, except CTP and $r_e$, which are in-cloud averages. In addition, CTP has been logarithmically averaged, while the other properties have been linearly averaged. Panel (a) shows the areas defined for the time series analysis in Fig. 10.

For CTP the agreement between the simulated model results and the retrievals is rather good over the Atlantic, while over land the modelled clouds have higher tops (lower CTP) than retrieved, even after the simulator has been applied. LWP patterns of simulator-retrieval differences are rather similar to those for TCF. These patterns can be roughly understood from the generally higher TCF and $\tau_c$ in the simulated model results over ocean, and the lower TCF and $r_e$ over land. The liquid $r_e$ plots reflect the simple parameterization of $r_e$ in the model, depending on fixed, and very different, aerosol concentrations over land and water (see Sect. 4.3). This results in a sharp land-sea gradient in the modelled/simulated $r_e$, with much smaller droplets over land. Since the $\tau_c$ for model layers is determined from liquid/ice water content and $r_e$, $\tau_c$ shows an opposite gradient with strongly enhanced $\tau_c$ values over land. Such features can be improved if actual aerosol data are introduced for the calculation of $r_e$. Apart from this land–sea artefact in $\tau_c$ related to $r_e$, the model also appears to overestimate LWP and liquid $\tau_c$ in particular near the western coasts of the continent.

## 6   Conclusions

A Cloud_cci satellite simulator has been developed to test the performance of model clouds compared to the new satellite CDR, Cloud_cci. In this study we have assessed certain aspects of cloudiness in the GCM EC-Earth and the RCM RACMO.

Firstly, the impact of using the simulator compared to just relying on the "native" model is shown using the TCF. In large areas more than $20\%$ of the cloud cover is reduced by the simulator through the process of removing thin clouds, although the average global reduction is around $10\%$. This is in line with the reality that the Cloud_cci retrievals tend to not detect clouds that are optically thinner than a global average of around $\tau_c = 0.2$. We also demonstrated the importance of sampling the model at the correct local time to match the EOT of the satellites used in the Cloud_cci CDR. As was illustrated with model LWP, large areas may have up to $50\%$ too much or too little LWP only due to sampling errors if the satellite overpass time has drifted by 4 hours or so, and this mainly impacts the areas with a large diurnal cycle. For this reason the simulator automatically samples the model at the EOT of the satellites used in the Cloud_cci CDR.

Overall EC-Earth produces much the same cloudiness as seen in observations, with some key differences. For instance, in the Tropics, the cloud tops are too low in the model, especially in the Central Pacific region, whereas over North Africa and the Arabian subcontinent the clouds in EC-Earth appear too high. However, the desert areas tend to be dominated by thin high clouds, a cloud type that tends to be biased low for Cloud_cci (Stengel et al., 2017). There are also very large differences between EC-Earth and Cloud_cci in terms of $r_e$.

The evaluation of RACMO indicates some biases with respect to the Cloud_cci data. In particular cloud amount is higher in the model over the northern Atlantic. In contrast, over continental Europe the modelled cloud amount is lower, and the modelled CTP is — even after a considerable enhancement implied by the simulator — lower than retrieved.

Overall, the results shown here convincingly demonstrate that a simulator is needed to make meaningful comparisons between modelled and retrieved cloud properties. It is promising to see that for (nearly) all cloud properties the simulator improves the agreement of the model with the satellite data.

*Geoscientific*
*Model Development*
Discussions

*Author contributions.* Salomon Eliasson is the main author. He wrote most of the article, carried out all the simulations of Cloud_cci from EC Earth data, and made comparisons to the Cloud_cci CDR. Jan Fokke and Erik van Meijgaard used the simulator on the RACMO model and co-wrote all the sections related to RACMO and their comparison to the observations. Ulrika Willén, who is a model developer for EC Earth provided valuable input from the climate modellers perspective. Martin Stengel and Karl Göran Karlsson provided the Cloud_cci CDR
5 and provided valuable input from this CDRs perspective. All co-authors provided valuable editing help in each iteration of the article

*Competing interests.* No competing interests

*Data availability.* Cloud_cci observational data can be downloaded from http://www.esa-cloud-cci.org/?q=data_download. The EC Earth
10 data can be attained from http://www.nextdataproject.it/?q=en/content/ec-earth-cmip5-data-extraction, and RACMO model data can be attained through https://www.projects.science.uu.nl/iceclimate/models/racmo.php.

*Code and data availability.* The simulator code itself is so far only available by contacting the authors.

# References

Balsamo, G., Beljaars, A., Scipal, K., Viterbo, P., van den Hurk, B., Hirschi, M., and Betts, A. K.: A Revised Hydrology for the ECMWF
15     Model: Verification from Field Site to Terrestrial Water Storage and Impact in the Integrated Forecast System, J. Hydrometeorol., 10,
    623–643, https://doi.org/10.1175/2008JHM1068.1, 2009.

Ban-Weiss, G. A., Jin, L., Bauer, S. E., Bennartz, R., Liu, X., Zhang, K., Ming, Y., Guo, H., and Jiang, J. H.: Evaluating clouds,
    aerosols, and their interactions in three global climate models using satellite simulators and observations, J. Geophys. Res., 119,
    https://doi.org/10.1002/2014JD021722, 2014.

20 Baró, R., Jiménez-Guerrero, P., Stengel, M., Brunner, D., Curci, G., Forkel, R., Neal, L., Palacios-Peña, L., Savage, N., Schaap, M., Tuccella,
    P., Denier van der Gon, H., and Galmarini, S.: Comparison of regional meteorology-chemistry models with satellite cloud products
    over Europe, Atmos. Chem. Phys. Discuss., pp. 1–31, https://doi.org/10.5194/acp-2018-114, https://www.atmos-chem-phys-discuss.net/
    acp-2018-114/, 2018.

Bechtold, P., Semane, N., Lopez, P., Chaboureau, J.-P., Beljaars, A., and Bormann, N.: Representing Equilibrium and Nonequilibrium Con-
25     vection in Large-Scale Models, JAS, 71, 734–753, https://doi.org/10.1175/JAS-D-13-0163.1, 2014.

Bodas-Salcedo, A., Webb, M. J., Bony, S., Chepfer, H., Dufresne, J.-L., Klein, S. A., Zhang, Y., Marchand, R., Haynes, J. M.,
    Pincus, R., and John, V. O.: COSP: satellite simulation software for model assessment, Bull. Amer. Met. Soc., 92, 1023–1043,
    https://doi.org/10.1175/2011BAMS2856.1, 2011.

Boussetta, S., Simarro, C., and Lucas, D.: Exploring EC-Earth 3.2-Beta performance on the new ECMWF Cray-Broadwell, 2016.

30 Bugliaro, L., Zinner, T., Keil, C., Mayer, B., Hollmann, R., Reuter, M., and Thomas, W.: Validation of cloud property retrievals with simulated
    satellite radiances: a case study for SEVIRI, Atmos. Chem. Phys., 11, 5603–5624, https://doi.org/10.5194/acp-11-5603-2011, 2011.

Chepfer, H., Bony, S., Winker, D., Chiriaco, M., Dufresne, J.-L., and Sèze, G.: Use of CALIPSO lidar observations to evaluate the cloudiness
    simulated by a climate model, Geophys. Res. Lett., 35, L15704, https://doi.org/10.1029/2008GL034207, 2008.

Clough, S. A., Shephard, M. W., Mlawer, E. J., Delamere, J. S., Iacono, M., Cady-Pereira, K., Boukabara, S., and Brown, P. D.:
35     Atmospheric radiative transfer modeling: a summary of the AER codes, J. Quant. Spectrosc. Radiat. Transfer, 91, 233–244,
    https://doi.org/10.1016/j.jqsrt.2004.05.058, 2005.

Eliasson, S., Buehler, S. A., Milz, M., Eriksson, P., and John, V. O.: Assessing observed and modelled spatial distributions of ice water path
    using satellite data, Atmos. Chem. Phys., 11, 375–391, https://doi.org/10.5194/acp-11-375-2011, 2011.

Giorgi, F. and Gutowski, W. J.: Regional Dynamical Downscaling and the CORDEX Initiative, Annu. Rev. Environ. Resour., 40, 467–490,
    https://doi.org/10.1146/annurev-environ-102014-021217, 2015.

5 Guan, B., Waliser, D. E., Li, J.-L. F., and da Silva, A.: Evaluating the impact of orbital sampling on satellite-climate model comparisons, J.
    Geophys. Res., 118, 1–15, https://doi.org/10.1029/2012JD018590, 2013.

Haynes, J. M., Marchand, R. T., Luo, Z., Bodas-Salcedo, A., and Stephens, G. L.: A Multipurpose Radar Simulation Package: QuickBeam,
    Bull. Amer. Met. Soc., pp. 1723–1727, https://doi.org/10.1175/BAMS-88-11-1723, 2007.

Hazeleger, W., Severijns, C., Semmler, T., Ştefănescu, S., Yang, S., Wang, X., Wyser, K., Dutra, E., Baldasano, J. M., Bintanja, R., Bougeault,
10     P., Caballero, R., Ekman, A. M. L., Christensen, J. H., van den Hurk, B., Jimenez, P., Jones, C., Kållberg, P., Koenigk, T., McGrath, R.,
    Miranda, P., van Noije, T., Palmer, T., Parodi, J. A., Schmith, T., Selten, F., Storelvmo, T., Sterl, A., Tapamo, H., Vancoppenolle, M.,
    Viterbo, P., and Willén, U.: EC-Earth: A Seamless Earth System Prediction Approach in Action, Bull. Amer. Met. Soc., 2010.

Heidinger, A. K., Foster, M. J., Walther, A., and Zhao, X.: The Pathfinder Atmospheres–Extended AVHRR Climate Dataset, Bull. Amer. Met. Soc., 95, 909–922, https://doi.org/10.1175/BAMS-D-12-00246.1, https://doi.org/10.1175/BAMS-D-12-00246.1, 2014.

15 Jakob, C. and Klein, S. A.: The role of vertically varying cloud fraction in the parametrization of microphysical processes in the ECMWF model, Q. J. R. Meteorol. Soc., 125, 941–965, https://doi.org/10.1002/qj.49712555510, 1999.

Jonkheid, B. J., Roebeling, R. A., and van Meijgaard, E.: A fast SEVIRI simulator for quantifying retrieval uncertainties in the CM SAF cloud physical property algorithm, ACP, 12, 10 957–10 969, https://doi.org/10.5194/acp-12-10957-2012, https://www.atmos-chem-phys. net/12/10957/2012/, 2012.

20 Karlsson, K.-G. and Devasthale, A.: Evaluation of 2018 revisions of ESA-CLOUD-CCI and ISCCP cloud climate data records by reference to CLARA-A2, PATMOS-x and CALIPSO-CALIOP results, submitted to Rem. Sens., 2018.

Karlsson, K.-G. and Håkansson, N.: Characterization of AVHRR global cloud detection sensitivity based on CALIPSO-CALIOP cloud optical thickness information: demonstration of results based on the CM SAF CLARA-A2 climate data record, Atmos. Meas. Tech., 11, 633–649, https://doi.org/10.5194/amt-11-633-2018, https://www.atmos-meas-tech.net/11/633/2018/, 2018.

25 Karlsson, K.-G., Anttila, K., Trentmann, J., Stengel, M., Meirink, J.-F., Devasthale, A., Hanschmann, T., Kothe, S., Jääskeläinen, E., Sedlar, J., Benas, N., van Zadelhoff, G. J., Schlundt, C., Stein, D., Finkensieper, S., Håkansson, N., and Hollmann, R.: CLARA-A2: the second edition of the CM SAF cloud and radiation data record from 34 years of global AVHRR data, Atmos. Chem. Phys., 17, 5809–5828, https://doi.org/10.5194/acp-17-5809-2017, https://www.atmos-chem-phys.net/17/5809/2017/, 2017.

Kay, J. E., Hillman, B. R., Klein, S. A., Zhang, Y., Medeiros, B., Pincus, R., Gettelman, A., Eaton, B., Boyle, J., Marchand, R., and Ackerman,
30 T. P.: Exposing Global Cloud Biases in the Community Atmosphere Model (CAM) Using Satellite Observations and Their Corresponding Instrument Simulators, J. Climate, 25, 5190–5207, https://doi.org/10.1175/JCLI-D-11-00469.1, 2012.

Keller, M., Fuhrer, O., Kröner, N., Lüthi, D., Schmidli, J., Stengel, M., Stöckli, R., and Schär, C.: The sensitivity of Alpine summer convection to surrogate climate change: An intercomparison between convection-parameterizing and convection-resolving models, Atmos. Chem. Phys. Discuss., pp. 1–21, https://doi.org/10.5194/acp-2017-504, https://www.atmos-chem-phys-discuss.net/acp-2017-504/, 2017.

35 Klein, S. A., Zhang, Y., Zelinka, M. D., Pincus, R., Boyle, J., and Gleckler, P. J.: Are climate model simulations of clouds improving? An evaluation using the ISCCP simulator, J. Geophys. Res., 118, 1–14, https://doi.org/10.1002/jgrd.50141, 2013.

Koenigk, T., Brodeau, L., and Graversen, R. G.: Arctic climate change in 21st century CMIP5 simulations with EC-Earth, Climate Dynamics, 40, 2719–2743, https://doi.org/10.1007/s00382-012-1505-y, 2013.

Lauer, A., Eyring, V., Righi, M., Buchwitz, M., Defourny, P., Evaldsson, M., Friedlingstein, P., de Jeu, R., de Leeuw, G., Loew, A., Merchant, C. J., Müller, B., Popp, T., Reuter, M., Sandven, S., Senftleben, D., Stengel, M., Roozendael, M. V., Wenzel, S., and Willén, U.: Benchmarking CMIP5 models with a subset of ESA CCI Phase 2 data using the ESMValTool, Rem. Sen. Env., 203, 9– 39, https://doi.org/10.1016/j.rse.2017.01.007, http://www.sciencedirect.com/science/article/pii/S003442571730007X, earth Observation
5 of Essential Climate Variables, 2017.

Lenderink, G. and Holtslag, A. A. M.: An updated length-scale formulation for turbulent mixing in clear and cloudy boundary layers, Q. J. R. Meteorol. Soc., 130, 3405–3427, https://doi.org/10.1256/qj.03.117, http://dx.doi.org/10.1256/qj.03.117, 2004.

Lohmann, U. and Neubauer, D.: The importance of mixed-phase clouds for climate sensitivity in the global aerosol-climate model ECHAM6-HAM2, Atmos. Chem. Phys. Discuss., pp. 1–32, https://doi.org/10.5194/acp-2018-97, https://www.atmos-chem-phys-discuss.
10 net/acp-2018-97/, 2018.

Martin, G. M., Johnson, D. W., and Spice, A.: The measurement and parameterization of effective radius of droplets in warm stratocumulus clouds, J. Atmos. Sci., 51, 1823–1842, https://doi.org/http://dx.doi.org/10.1175/1520-0469(1994)051<1823:TMAPOE>2.0.CO;2, 1994.

McGarragh, G. R., Poulsen, C. A., Thomas, G. E., Povey, A. C., Sus, O., Stapelberg, S., Schlundt, C., Proud, S., Christensen, M. W., Stengel, M., Hollmann, R., and Grainger, R. G.: The Community Cloud retrieval for CLimate (CC4CL) – Part 2: The optimal estimation approach,

15     Atmospheric Measurement Techniques, 11, 3397–3431, https://doi.org/10.5194/amt-11-3397-2018, https://www.atmos-meas-tech.net/11/3397/2018/, 2018.

Mlawer, E. J., Taubman, S. J., Brown, P. D., Iacono, M. J., and Clough, S. A.: Radiative transfer for inhomogeneous atmospheres: RRTM, a validated correlated-k model for the longwave, J. Geophys. Res., 102, 16 663–16 682, 1997.

Morcrette, J.-J., Barker, H. W., Cole, J. N. S., Iacono, M. J., and Pincus, R.: Impact of a New Radiation Package, McRad, in the ECMWF

20     Integrated Forecasting System, MWR, 136, 4773–4798, https://doi.org/10.1175/2008MWR2363.1, 2008.

Noda, A. T. and Satoh, M.: Intermodel variances of subtropical stratocumulus environments simulated in CMIP5 models, Geophys. Res. Lett., 41, 7754–7761, https://doi.org/10.1002/2014GL061812, 2014.

Norris, J. R., Allen, R. J., Evan, A. T., Zelinka, M. D., O'Dell, C. W., and Klein, S. A.: Evidence for climate change in the satellite cloud record, Nature, 536, 72–75, https://doi.org/10.1038/nature18273, 2016.

25   Pincus, R., Platnick, S., Ackerman, S. A., Hemler, R. S., and Hofmann, R. J. P.: Reconciling Simulated and Observed Views of Clouds: MODIS, ISCCP, and the Limits of Instrument Simulators, J. Climate, 25, 4699–4720, https://doi.org/10.1175/JCLI-D-11-00267.1, 2012.

Rodgers, C. D.: Inverse methods for atmospheric sounding : theory and practice, Singapore ; [River Edge, N.J.] : World Scientific, c2000, 2009.

Roebeling, R. A. and van Meijgaard, E.: Evaluation of the daylight cycle of model-predicted cloud amount and condensed water path over

30     Europe with observations from MSG SEVIRI, J. Climate, 22, 1749–1766, https://doi.org/10.1175/2008JCLI2391.1, 2009.

Sassen, K., Wang, Z., and Liu, D.: Global distribution of cirrus clouds from CloudSat/Cloud-Aerosol Lidar and Infrared Pathfinder Satellite Observations (CALIPSO) measurements, J. Geophys. Res., 113, 1–12, https://doi.org/10.1029/2008JD009972, 2008.

Siebesma, A. P., Soares, P. M. M., and ao Teixeira, J.: A Combined Eddy-Diffusivity Mass-Flux Approach for the Convective Boundary Layer, J. Atmos. Sci., 64, 1230–1248, https://doi.org/10.1175/JAS3888.1, 2007.

35   Song, H., Zhang, Z., Ma, P., Ghan, S., and Wang, M.: An Evaluation of Marine Boundary Layer Cloud Property Simulations in Community Atmosphere Model Using Satellite Observations: Conventional Sub-grid Parameterization vs. CLUBB, J. Climate, https://doi.org/10.1175/JCLI-D-17-0277.1, in press, 2017.

Stengel, M., Mieruch, S., Jerg, M., Karlsson, K.-G., Scheirer, R., Maddux, B., Meirink, J.-F., Poulsen, C., Siddans, R., Walther, A., and Hollmann, R.: The Clouds Climate Change Initiative: Assessment of state-of-the-art cloud property retrieval schemes applied to AVHRR heritage measurements, Remote Sensing of Environment, 162, 363 – 379, https://doi.org/https://doi.org/10.1016/j.rse.2013.10.035, http://www.sciencedirect.com/science/article/pii/S0034425713004197, 2015.

5   Stengel, M., Stapelberg, S., Sus, O., Schlundt, C., Poulsen, C., Thomas, G., Christensen, M., Carbajal Henken, C., Preusker, R., Fischer, J., Devasthale, A., Willén, U., Karlsson, K.-G., McGarragh, G. R., Proud, S., Povey, A. C., Grainger, R. G., Meirink, J. F., Feofilov, A., Bennartz, R., Bojanowski, J. S., and Hollmann, R.: Cloud property datasets retrieved from AVHRR, MODIS, AATSR and MERIS in the framework of the Cloud_cci project, Earth Syst. Sci. Data, 9, 881–904, https://doi.org/10.5194/essd-9-881-2017, 2017.

Stengel, M., Schlundt, C., Stapelberg, S., Sus, O., Eliasson, S., Willén, U., and Meirink, J.-F.: Comparing ERA-Interim clouds

10     with satellite observations using a simplified satellite simulator, Atmospheric Chemistry and Physics Discussions, 2018, 1–22, https://doi.org/10.5194/acp-2018-258, https://www.atmos-chem-phys-discuss.net/acp-2018-258/, in Review, 2018.

Stephens, G. L.: Radiation Profiles in Extended Water Clouds. II: Parameterization Schemes, J. Atmos. Sci., 35, 2123–2132, 1978.

Stephens, G. L., Vane, D. G., Boain, R. J., Mace, G. G., Sassen, K., Wang, Z., Illingworth, A. J., O'Connor, E. J., Rossow, W. B., Durden, S. L., Miller, S. D., Austin, R. T., Benedetti, A., Mitrescu, C., and the CloudSat Science Team: The CloudSat mission and the A-train, Bull. Amer. Met. Soc., 83, 1771–1790, 2002.

Stocker, T. F., Qin, D., Plattner, G.-K., Tignor, M., Allen, S., Boschung, J., Nauels, A., Xia, Y., Bex, V., and (eds.), P. M.: IPCC, 2013: Climate Change 2013: The Physical Science Basis. Contribution of Working Group I to the Fifth Assessment Report of the Intergovernmental Panel on Climate Change, Cambridge University Press, Cambridge, United Kingdom and New York, NY, USA, www.climatechange2013.org, 2013.

Sun, F., Hall, A., and Qu, X.: On the relationship between low cloud variability and lower tropospheric stability in the Southeast Pacific, Atmos. Chem. Phys., 11, 9053–9065, https://doi.org/10.5194/acp-11-9053-2011, 2011.

Sus, O., Stengel, M., Stapelberg, S., McGarragh, G., Poulsen, C., Povey, A. C., Schlundt, C., Thomas, G., Christensen, M., Proud, S., Jerg, M., Grainger, R., and Hollmann, R.: The Community Cloud retrieval for CLimate (CC4CL) – Part 1: A framework applied to multiple satellite imaging sensors, Atmospheric Measurement Techniques, 11, 3373–3396, https://doi.org/10.5194/amt-11-3373-2018, https://www.atmos-meas-tech.net/11/3373/2018/, 2018.

Swales, D. J., Pincus, R., and Bodas-Salcedo, A.: The Cloud Feedback Model Intercomparison Project Observational Simulator Package: Version 2, Geosci. Model Dev., 11, 77–81, https://doi.org/10.5194/gmd-11-77-2018, https://www.geosci-model-dev.net/11/77/2018/, 2018.

Tan, J., Oreopoulos, L., Jakob, C., and Jin, D.: Evaluating rainfall errors in global climate models through cloud regimes, Climate Dynamics, https://doi.org/10.1007/s00382-017-3806-7, https://doi.org/10.1007/s00382-017-3806-7, 2017.

Terai, C. R., Klein, S. A., and Zelinka, M. D.: Constraining the low-cloud optical depth feedback at middle and high latitudes using satellite observations, JGR, 121, 9696–9716, https://doi.org/10.1002/2016JD025233, http://dx.doi.org/10.1002/2016JD025233, 2016.

Tiedtke, M.: A comprehensive mass flux scheme for cumulus parametrization in large-scale models, Mon. Weather Rev., 117, 1779–1800, 1989.

Tiedtke, M.: Representation of clouds in large-scale models, Mon. Weather Rev., 121, 3040–3061, 1993.

Tompkins, A. M., Gierens, K., and Rädel, G.: Ice supersaturation in the ECMWF integrated forecast system, Tech. rep., European Centre for Medium-Range Weather Forecasts ECMWF,Technical Memorandum, https://doi.org/10.1002/qj.14, 2007.

Unden, P., Rontu, L., Järvinen, H., Lynch, P., Calvo, J., Cats, G., Cuxart, J., Eerola, K., Fortelius, C., Garcia-Moya, J. A., Jones, C., Geert, Lenderlink, G., Mcdonald, A., Mcgrath, R., Navascues, B., Nielsen, N. W., Degaard, V., Rodriguez, E., Rummukainen, M., Sattler, K., Sass, B. H., Savijarvi, H., Schreur, B. W., Sigg, R., and The, H.: HIRLAM-5 Scientific Documentation, 2002.

van den Hurk, B., Siegmund, P., (Eds), A. K. T., Attema, J., Bakker, A., Beersma, J., Bessembinder, J., Boers, R., Brandsma, T., van den Brink, H., Drijfhout, S., Eskes, H., Haarsma, R., Hazeleger, W., Jilderda, R., Katsman, C., Lenderink, G., Loriaux, J., van Meijgaard, E., van Noije, T., van Oldenborgh, G.-J., Selten, F., Siebesma, P., Sterl, A., de Vries, H., van Weele, M., de Winter, R., and van Zadelhoff, G.-J.: Climate Change scenarios for the 21st Century – A Netherlands perspective, Tech. rep., http://www.climatescenarios.nl, scientific Report WR2014-01, 2014.

van Meijgaard, E., van Ulft, L. H., Lenderink, G., de Roode, S., Wipfler, L., Boers, R., and Timmermans, R. M. A.: Refinement and application of a regional atmospheric model for climate scenario calculations of Western Europe, Tech. rep., KNMI, De Bilt, The Netherlands, http://climexp.knmi.nl/publications/FinalReport_KvR-CS06.pdf, climate changes Spatial Planning publication: KvR 054/12, 2012.

Voors, R., Donovan, D., Acarreta, J., Eisinger, M., Franco, R., Lajas, D., Moyano, R., Pirondini, F., Ramos, J., and Wehr, T.: ECSIM: the simulator framework for EarthCARE, vol. 6744 of *Proceedings of SPIE*, 2007.

Waliser, D. E., Li, J.-L. F., Woods, C. P., Austin, R. T., Bacmeister, J., Chern, J., Genio, A. D., Jiang, J. H., Kuang, Z., Meng, H., Minnis, P., Platnick, S., Rossow, W. B., Stephens, G. L., Sun-Mack, S., Tao, W.-K., Tompkins, A. M., Vane, D. G., Walker, C., and Wu, D.: Cloud ice: A climate model challenge with signs and expectations of progress, J. Geophys. Res., 114, D00A21, https://doi.org/10.1029/2008JD010015, 2009.

Webb, M., Senior, C., Bony, S., and Morcrette, J.-J.: Combining ERBE and ISCCP data to assess clouds in the Hadley Centre, ECMWF and LMD atmospheric climate models, Climate Dynamics, 17, 902–922, https://doi.org/10.1007/s003820100157, 2001.

Webb, M. J., Andrews, T., Bodas-Salcedo, A., Bony, S., Bretherton, C. S., Chadwick, R., Chepfer, H., Douville, H., Good, P., Kay, J. E., Klein, S. A., Marchand, R., Medeiros, B., Siebesma, A. P., Skinner, C. B., Stevens, B., Tselioudis, G., Tsushima, Y., and Watanabe, M.: The Cloud Feedback Model Intercomparison Project (CFMIP) contribution to CMIP6, Geosci. Model Dev., 10, 359–384, https://doi.org/10.5194/gmd-10-359-2017, https://www.geosci-model-dev.net/10/359/2017/, 2017.

Winker, D. M., Vaughan, M. A., Omar, A., Hu, Y., Powell, K. A., Liu, Z., Hunt, W. H., and Young, S. A.: Overview of the CALIPSO Mission and CALIOP Data Processing Algorithms, J. Atmos. Oceanic Technol., 26, 2310–2323, https://doi.org/10.1175/2009JTECHA1281.1, 2009.

Young, A. H., Knapp, K. R., Inamdar, A., Hankins, W., and Rossow, W. B.: The International Satellite Cloud Climatology Project H-Series climate data record product, Earth Syst. Sci. Data, 10, 583–593, https://doi.org/10.5194/essd-10-583-2018, https://www.earth-syst-sci-data.net/10/583/2018/, 2018.

Zelinka, M. D., Randall, D. A., Webb, M. J., and Klein, S. A.: Clearing clouds of uncertainty, Nature Clim. Change, 7, 674–678, 2017.

Zhang, M. H., Lin, W. Y., Klein, S. A., Bacmeister, J. T., Bony, S., Cederwall, R. T., Del Genio, A. D., Hack, J. J., Loeb, N. G., Lohmann, U., Minnis, P., Musat, I., Pincus, R., Stier, P., Suarez, M. J., Webb, M. J., Wu, J. B., Xie, S. C., Yao, M.-S., and Zhang, J. H.: Comparing clouds and their seasonal variations in 10 atmospheric general circulation models with satellite measurements, J. Geophys. Res., 110, D15S02, https://doi.org/10.1029/2004JD005021, 2005.

**Appendix: Glossary**

$\tau_c$  visible cloud optical depth at 550nm. 5–8, 12, 13, 16, 18, 24, 25

$r_e$  cloud particle effective radius. 5, 7, 8, 21, 24, 25

**AATSR**  Advanced Along-Track Scanning Radiometer. 2

**AMIP**  Atmospheric Model Inter-comparison Project. 4

**AVHRR**  Advanced Very High Resolution Radiometer. 2, 4–6, 9, 10

**CALIOP**  Cloud-Aerosol Lidar with Orthogonal Polarisation. 2, 3, 13

**CC4CL**  Community Cloud Retrieval for Climate. 5

**CDR**  Climate Data Record. 1–12, 14, 16, 18–23, 25, 26

**Geoscientific**
**Model Development**
Discussions

**ISCCP** International Satellite Cloud Climatology Project. 2, 3, 16

**ITCZ** Inter-Tropical Convergence Zone. 16

650 **IWP** Ice Water Path. 8

**JJA** June, July, and August. 12–14, 16

**KNMI** Koninklijk Nederlands Meteorologisch Instituut. 1, 5

**LWP** Liquid Water Path. 8, 9, 11, 13, 22–25

**MISR** Multiangle Imaging SpectroRadiometer. 2

655 **MODIS** MODerate resolution Imaging Spectroradiometer. 2, 3, 6–8, 16

**NOAA** National Oceanic and Atmospheric Administration. 5, 11

**NWP** Numerical Weather Prediction. 4

**OE** Optimal Estimation. 2, 5

**PATMOS-x** Pathfinder Atmospheres- Extended. 2

660 **RACMO** Regional Atmospheric Climate Model. 1, 4–7, 21–23, 25

**RCM** Regional Climate Model. 4, 22, 25

**RRTM** Rapid Radiation Transfer Module. 4

**SEVIRI** Spinning Enhanced Visible Infra-Red Imager. 3

**SIMFERA** SIMplistic cloud simulator For ERA-interim. 6

665 **SMHI** Swedish Meteorological and Hydrological Institute. 1

**SST** Sea Surface Temperature. 4

**TCF** Total Cloud Fraction. 1, 12–14, 22, 23, 25

**TESSEL** Tiled ECMWF Scheme for Surface Exchanges over Land. 4

**TKE** Turbulence Kinetic Energy. 4

670 **TOA** Top of Atmosphere. 7

**TWP** Tropical Warm Pool. 19

**UTC** Coordinated Universal Time. 5

**VIS** Visible. 2, 3